Author response to Referee #1

Update submitted along with the revised manuscript

We would like to thank the referee for taking the time to review our manuscript and for providing thoughtful and substantial feedback, which we are sure will help us to substantially improve the manuscript.

In the following, reviewer comments are typeset in black, authors' answers (A) in blue, and realized modifications (M) in green.

Anonymous Referee #1

1 General comments

The present manuscript is a solid compilation of results of geophysical measurements of two karst lakes in Mexico. The paper is well structured and the reader gets detailed insights into the extensive measurements with different geophysical methods. However, the paper strongly reminds of a project report. In my opinion a scientific paper in SE should go beyond a case study (maybe even with a more interesting title?). First, I would like to know more about the authors' motivation why this kind of lakes should be studied. In the introduction it is mentioned that it could be about choosing a suitable drilling location. This is not further discussed in the paper. I lack the approach how these results can be transferred to other locations / problems. On the other hand, the fact that these karst lakes are falling dry is an extremely interesting point. Finally, this offers the geophysicists the possibility to repeat the measurements with a "covered" layer and to verify the results. This could be emphasized much more in the paper. The topic has much more potential to serve not only as a method comparison or case study.

A: More interesting title

M: New title: "Integrated land and water-borne geophysical surveys shed light on the sudden drying of large karst lakes in southern Mexico"

A: Motivation to study this kind of lakes

We agree with the reviewer that besides the mere possibility to test a multi-methodological survey approach for the geophysical investigation of lakes, our motivation to study this kind of lakes remains unclear.

In general, the adaptation of geophysical techniques for the investigation of karst lakes is of relevance, given that ground and surface water in karst areas may react very sensible to even smaller variations of climatic conditions (e.g., precipitation, temperature, etc.). About 10% of the world's continental area is covered by karst and up to one quarter of the earth`s population at least partly depends on drinking water from karst aquifer systems (e.g., Hartmann et al., 2014). Thus, karst water management will be important in the future and require reliable geological information. Where geological drillings are not available to obtain this information directly, geophysical methods have been used successfully to explore the subsurface of karst systems (Bechtel et al., 2007). Karst lakes are often in direct contact with the aquifer via karst conduits, which results in an increased vulnerability of both water bodies. This motivates the search for new, complementary geophysical exploration methods, which can be applied on land and on the water.

At the same time, paleoenvironmental studies, e.g. based on the analysis of lake sediments, can help to better understand the impact of a changing climate on karst systems. By extracting information on past variations from the sedimentary record of lakes, these studies shed light on the local links between climate and availability and quality of water of karst lakes and the connected karst aquifer. In order to obtain a continuous paleoenvironmental record, which goes as far back into the past as possible, the drilling sites for the extraction of lakes sediments have to be carefully selected. Detailed information on the sedimentary infill of the lakes, in particular on thickness, composition, and possible perturbations, helps to find a suitable location. Thus, a geophysical survey, which is able to provide such information, can greatly contribute to the success of the paleoenvironmental approach.

Field-observations and paleoenvironmental studies from the study area indicate that large seasonal lake-level variations are part of the nature of the lakes and even "catastrophic" events such as the one observed in 2019 might be recurrent (with a period >50 years). Thus, urgent questions in the study area are whether the sudden drainage of 2019 could be linked to recent climate change and whether it is possible that such events will occur more frequently in the future. Besides the ongoing paleoenvironmental investigation, a comprehensive geological picture of the lakes´ geological substructure is essential to discuss possible draining mechanisms and their triggers.

Based on these considerations, the present geophysical study has three main objectives: (1) Determine suitable drilling locations to obtain complete, undisturbed, and far-reaching sedimentary sequences for paleoenvironmental studies, (2) provide basic knowledge on the geological substructure of the lakes (distribution and thickness of sediment cover, distribution of bare limestone rock with possible connectivity with the karst aquifer, etc.), and (3) adapt and test a multi-methodological geophysical approach to achieve the first two objectives.

M: We included this extended motivation into the revised version of the introduction of our manuscript, where we also clearly state the three main objectives of the survey. Corresponding adaptations were made in the abstract, too.

Along with the corresponding changes, we removed the references to Cohuo et al. (2018), Pérez et al. (2011), and Sigala et al. (2017) and included new references to Vázquez-Molina et al. (2016), Pérez et al, (2020), Medina-Elizalde and Rohling (2012), Echeverría Galindo et al. (2019), and Charqueño Celis et al. (2019).

A: Further discuss search for drilling location

After having broadened the scope of the manuscript as sketched above, we will also discuss the selection of drilling sites as well as the geological information provided by the geophysical survey and its implications in more detail.

Based the results discussed so far, the thick (5-6 m according to the SBP image) and apparently undisturbed fine-grained lacustrine sediments along Profile 1 (between 450 and 550 m, as well as between 600 and 700 m) lend themselves for a successful paleolimnological perforation. A perforation at these sites would also have the potential to shed light on the real nature of the second layer and either verify or falsify our interpretation as debris-sediment mixture. With a thickness of >50 m according to our electrical imaging results, the sedimentary cover along Profile 5 of Lake Tzibaná is thicker than the sediments of Lake Metzabok. However, our results also show that much of these sediments rather correspond to fluvial deposits of the river delta. In this depositional regime, we expect much higher rates of sedimentation, such that the mere sediment thickness does not necessarily imply an older record. In addition, a river delta is a much more complex system, in

which sediments can be deposited, eroded, and redeposited repeatedly, which decreases the probability to obtain undistorted sediment records as encountered further offshore.

Or field observations and geophysical results also have implications for the general understanding of the geological setting of the two studied lakes. Obviously, large areas of Lake Metzabok are covered by a layer of fine-grained (clayey) sediments, which – in these areas – is sufficiently thick to act as a hydrological barrier between the lake and the surrounding and underlying karst. However, the remaining heavily fractured and uncovered limestone outcrops effectively connect the lake with the karst system. This conclusion is underscored by the velocity at which the two lakes drained practically simultaneously between February and July 2019. During this time, the water loss amounted to 28,000 m^3/day or 0.3 m^3/s on average (Matti Altmann, personal communicatioin), which corresponds to the discharge of a large creek (e.g., McManamay and DeRolph, 2018).

While the interconnectivity between surface water and karst aquifer is well documented by field observations and further underpinned by our geophysical results, the actual mechanism as well as the cause of the sudden drainage remain unrevealed. The suddenness of the drainage (onset of discharge in the first days of February derived from satellite-image time series, Altmann, personal communication), indicates that one or more previously clogged karst conduits were unplugged around these dates. Planned time-series analyses of hydrological (e.g., lake water levels from satellite data) and meteorological data (precipitation, temperature, etc.) in combination with paleoenvironmental studies on sediment cores will possibly provide more hints on the mechanism and its triggers, and thus shed light on the question whether the drainage is influenced by climate variations.

M: We included and further extended this discussion as a new section “5.1 Identification of suitable drilling locations” into the revised version of our manuscript.

A: Transfer of results to other locations and problems

We consider the discussion of the combined application and interpretation of various geophysical methods on the two karst lakes itself a relevant reference for similar surveys at other locations. However, we agree with the reviewer in so far as the general importance of our findings can be developed in more detail.

M: Reviewer 2 suggested to provide a table that summarizes the used methods, as well as their advantages and limitations. Based on this table, we rewrote large parts of the discussion section under the new subsection title “5.3 Lessons learned from implementing a multi-methodological approach for lake-bottom reconnaissance”.

A: Emphasize more the fact that lakes fall dry and the positive implications for geophysics

M: As suggested, in the revised version of the manuscript, we put more emphasis on the positive implications of the drainage for our geophysical investigations. The occurrence of this event has really provided us with a unique opportunity to “repeat” measurements without a removed cover layer of up to 20 m water.

A: Not only method comparison or case study

We agree that study and topic have more potential.

M: We took advantage of this potential by extending the scope of the manuscript as sketched above.

2 Specific comments

• Chapter 3 deals in great detail with data acquisition and processing. All measurements of the applied wave and potential methods are clearly explained. In this as well as in the chapters 4 and 5 the insufficient signal-to-noise ratio is pointed out for some configurations. However, when evaluating the results, the reader is left in the dark when it comes to quantifying the error influences. This is an issue that urgently needs to be addressed - how much data could be included into the inversion process compared to the amount of measured data. How can the errors of the obtained models be estimated? (Example in line 182 - mean picking percents is ...)

M: We now describe the error and processing of TEM, TDIP, and SRT data in more detail and included exemplary data and error visualizations in a new appendix. Data quality and its general implications for the depth of investigation are also discussed in more detail. The model misfit of the final inverted models was included into all figures showing imaging results.

• Is it possible that sample TSI19-A is influenced by higher limestone content? This would support the latter interpretation of field measurement results.

A: A more detailed laboratory analysis of the sediment samples is still underway. Thus, we have not yet been able to understand the obvious deviation of the TDIP response of sample TSI19-A.

Preliminary results do not indicate a different mineralogical composition of sample TSI19-A compared to the rest of the samples. X-ray powder diffraction analyses show similar concentrations of dolomite (calcium magnesium carbonate) and calcite (calcium carbonate) in all six samples. However, the geochemical analysis does show a significantly increased total organic carbon (TOC) and carbon-to-nitrogen ratio (C/N) of the sample TSI19-A compared to the other five samples. Together, the high levels of these two parameters point to a larger fraction of organic matter from terrestrial sources (i.e., land-based plants), while the smaller amount of organic matter of the other five samples probably stems from algal plants.

Both samples TSI19-A and TSI19-B were collected on the exposed delta of the Nahá river. However, the location TSI19-A seems to have received more fluvial deposits due to its position closer to the estuary of the river, while location TSI19-B corresponds to a residual body water (i.e., in a predominantly aquatic environment) situated within the delta. In fact, in Figure 9, we can see that TSI19-A is located on the northernmost extension of the unit labelled as fluvial deposits, while TSI19-B is located in a (partly water-filled) depression underlain by the fine-grained (clayey) lake sediments. Thus the deviation of the TDIP response of sample TSI19-A is rather linked to the source of the sediment (fluvial vs. lacustrine) than to its mineralogical composition (e.g., limestone content) as might be assumed based in the TDIP field survey, where particularly higher phase responses can be related to the limestone bedrock.

M: We included a summary of this discussion into the revised manuscript in order to make clear that the higher phase and resistivity values of the sample TSI19-A are rather related to the depositional regime than the limestone content.

• In Line 214 ff. you mentioned underlain collapsed blocks - did you see some hints after the lakes are fallen dry?

A: The (few) uncovered limestone outcrops show both highly fractured limestone as well as limestone debris. However, the presence of limestone debris below the (thick) sediment cover has not been validated independently in the field. Thus, the underlying collapsed bedrock is clearly an interpretation, which is solely based on (i) a reasonable conceptual model of the evolution of the

lakes from collapsed bedrock and (ii) the layered resistivity structure below the flat sediment-filled parts of lake Metzabok (pure sediments, sediment-debris mixture, bedrock).

M: We included an additional Figure (Fig. 8b-d, revised manuscript) showing superficial expressions of the interpreted geological units, in particular the limestone debris and the fractured limestone.

• Line 229 and Fig. 4f: you do not interpret phase values for depth gt 50 m (due to insufficient data quality, ok - see first comment in list!), but than you should avoid to show this part of inversion model - it is more than the half of the picture!

M: We blanked less sensitive areas (cumulative normalized sensitivity smaller than 1/100 of the largest sensitivity) of all TDIP imaging results and adjusted the maximum depths of the corresponding figures accordingly.

• I am amazed by the variety of methods and the integrative approach for this survey. Only the complementary methods produce a comprehensive geological model. I would not use chapter 5.3 as a confrontation of methods (title: seismic vs electrical methods) but rather promote these complementary techniques as a great advantage, the usage of the methods depends on the given situation and problem!

M: We removed section “5.3 Seismic vs. electrical methods” and reorganized the entire part of the discussion section dealing with the evaluation of the individual methods. We also highlight the advantage of using complementary methods and data to obtain a comprehensive geological model.

• Chapter conclusion should pick up some information from the introduction and give a broader (more general) summary at the end - how about the drilling, what is the take home message?

M: As suggested, the revised conclusion section became broader and more general summary. In particular, we will include conclusive statements regarding the findings with respect to a more general geological interpretation (also suggested by the second reviewer), the selection of drilling locations for paleoenvironmental studies, and the lessons learned from the evaluation of the individual methods.

3 Technical Corrections

The pictures are generally of very good quality. Sometimes it is a bit confusing to recognize the correct position of the subprofiles (There are also different names for one and the same profile - to much information: example profile 1 aka L4NS aka MET19-1 MET19-2). Especially in Figure 5 it would help to use the same coordinates as in figure 4 (even if the profiles have an 10 m offset in EW direction). In Figure 4 the TDEM is slightly shifted in comparison to SBP.

M: We removed the labels referring to the IDs of the data set published along with the manuscript (e.g., L4NS, MET19-1, etc.). In the revised version of the manuscript, in Figure 5, we use the same coordinates as in Figure 4. The TDIP images in Figures 4f and 4g have an offset of about 25 m with respect to the SBP profile in Figure 4e. We included dotted arrows to indicate the position of the TDIP profile with respect to the SBP image.

Additional references for this author response (all other references included in the manuscript)

McManamay, R. A., & DeRolph, C. R. (2019). A stream classification system for the conterminous United States. Scientific data, 6, 190017.

Author response to Referee #2 (Pritam Yogeshwar, University of Cologne)

Update submitted along with the revised manuscript

Thank you, Pritam, for taking your time to review our manuscript and for your detailed and constructive feedback – especially on the TEM method – which we will surely help us to improve the manuscript a lot!

In the following, reviewer comments are typeset in black, authors' answers (A) in blue, and planned modifications (M) in green.

Pritam Yogeshwar (Referee)

yogeshwar@geo.uni-koeln.de

1. General Comments

I have carefully and interestingly read and reviewed the manuscript (MS). The authors present an interesting multi-method case study on two lakes in Mexico using water borne geophysics. Especially the sudden lake water level drop as well as the application of multiple methods are highlights of this study. The results are very well prepared and technically on a high level. Besides my positive impression, there are a few points to be addressed.

The authors present studies on two lakes - Metzabok and Tzibana. If feasible, I suggest to incorporate some more general discussion on how these lakes are connected. Are there any general conclusions/interpretations that apply to both lakes or is it even possible to connect the subsurface structure? For example, there is no clay interpreted in lake Metzabok whereas major parts of the subsurface in lake Tzibana is related to clay rich sediments.

A: We agree. Resulting from the very limited information provided on Lake Tzibaná, it does not become clear, how the two neighboring lakes are connected. The new Fig. 9 of the revised manuscript shows the result of one long SBP transect crossing Lake Tzibaná and the delta of the Nahá river from North to South. From this line, it becomes clear that outside the delta with it sandy sediments, the deeper part of Lake Tzibaná shows a similar geology as Lake Metzabok (flat sediment-covered lake bottom). However, the flat parts of Lake Tzibaná, which are expected to be more comparable with Metzabok, are much deeper than Metzabok and were also not accessible (still water covered) during the second field season, such that no additional data could be collected directly on the lake bottom.

M: We included a new SBP profile in the revised version of the manuscript and provide a more complete discussion of the common features and differences between the two studied lakes.

It is not easy to find a red line in the MS. This is partly due to the fact that all profiles on lake Metzabok are discussed one by one. And, subsequently the results for lake Tzibana are shown. I suggest to strengthen the explicit motivation why both studies were performed. Possibly a road-map can be formulated indicating why which method was used and how the survey was designed to address the scientific questions. As I understand the study aims at few aspects (1) detect depth to bedrock (2) understand sudden lake level drop and related subsurface conditions such as Karst collapse and (3) combined interpretation of various methods (especially TD-IP phase data evaluation for the first time in sedimentary studies).

A: We agree. The focus of the manuscript in its current form is the comparison of methods, which is developed and discussed step by step along the profiles. Both received reviews demand for a broadening of the scope by improving the description of the more general scientific motivation and the inclusion of a more rigorous geological/hydrogeological contextualization.

M: In response to these suggestions, we reworked the abstract, the introduction section, the discussion section, and the conclusions. We explicitly include a "road-map" similar to the one suggested here.

I suggest to elaborate more on the benefit of using TD-IP and evaluating the phase data for the two lake studies, since this is not very common. If feasible elaborate more in detail how the phase data relates to subsurface physical properties in general.

A: We also see the benefit of discussing the IP response of lake sediments in more detail.

M: Mainly guided by the question of Reviewer 1, whether the sample TSI19-A might contain a larger fraction of limestone, we extended our discussion of the IP response of lake sediments in the results and interpretation section and the discussion section.

2. Specific comments

• I understand that the focus is on the geoscientific interpretation using a multidisciplinary approach. However, I do miss some technical aspects of the study with respect to method and inversion. For example, some typical survey parameters (e.g. anchored or continuous TEM system; typical measurement errors).

A: We recognize that we might have overshot the target of providing very brief descriptions of the various methods used in this multi-method survey. In the following, we provide some additional information on the TEM measurement setup and the inversion approach.

During the survey, the TEM system was towed from station to station. The electromotor of the rubber boat was only used for navigation between sounding locations and remained turned off during the measurements themselves. Because we did not use any anchors, depending on the wind conditions at the sounding sites, the loop slowly drifted during the measurements resulting in maximum estimated displacements of 1 – 2 times the loop diameter (i.e., ~40 m).

For the transient length of 1024 µs used for our measurements, the TEM-FAST48 records 64 transients, which are analogously averaged by the hardware. For one sounding measurement, this basic measuring cycle is repeated $n \times 13$ times. For $n = 4$ (our measurements), this results in 52 repetitions of the basic cycle (and a total of 3328 effective stacks), which are used to compute the impulse response by digital averaging and to determine the measurement error as the standard error of the mean (SEM). As the exemplary data the new Figure A1 shows, for the latest time gates used for the inversion (around 200 µs), the SEM is $\lesssim 2 \cdot 10^{-6}$ V/A (or $\lesssim 5 \cdot 10^{-9}$ V/Am²).

We use the conventional 1D smoothness-constraint inversion approach implemented in the software ZondTEM1d (Kaminsky, personal communication) to interpret the TEM soundings. The software supports arbitrary shaped loops, the vertices of which can be defined independently for transmitter and receiver. This warrants a correct interpretation of our coincident loop transient data. While our measurements were carried out with a circular loop (transmitter and receiver) of 22.9 m diameter (area 412 m²), we use a square loop of equal area (20.4 m x 20.4 m) in the inversion.

M: We added the above listed details on the TEM data and inversion to the methods sections and the new appendix.

Moreover, there is currently no data visualized (Only the TD-IP lab data). I suggest to include a section with data, and possibly also with inversion model response (If feasible, for example in an appendix). Of course this should not distract from the study itself.

A: We see the importance of including visualizations of exemplary data and inversion model responses (as an appendix) in order to allow the interested reader to quickly gain an impression of data quality and inversion model fits. Besides this new appendix, all data, inverted models and computed responses will still be available from the open data repository and can be revised there in detail.

M: We added an appendix to show exemplary data and inversion model responses for TEM, TDIP, and SRT measurements.

• From my experience, the TEMfast device sometimes shows significant distortions using small loop configurations. Did you observe any data distortions especially since a very small configurations was used? And, did you for example compare some land based soundings using a larger transmitter to validate that the very small layout gives correct transient data? In this respect, I also suggest to show at least some data.

A: The new Fig. A1 shows measured and calculated apparent resistivity curves of 5 soundings along TEM Profile 5 of Lake Tzibaná (smooth and layered resistivity models shown in Figure 10 of the manuscript). The measured curves are well recovered by the inverted models and do not show any conspicuous features, which would point to a distortion (e.g., due to the small loop configuration).

We have not carried out test measurements with different loop sizes during the field work in Mexico. But we do have some test measurements at different locations in Europe: Figure R2.4 shows the impulse responses for single-loop measurements with 4 different sizes of the square loop (6, 12, 25, and 50 m). For times >10 µs, all loop sizes result in consistent transients without conspicuous distortions. In particular, the same applied for the uniform time window between 20 and 200 µs, to which our transients from the Mexican lakes were truncated. It is worth mentioning that the average resistivity of the test location (approx. 120 Ωm across the first 50 m) is slightly larger than the average resistivity in the lake environment (20-30 Ωm). However, from our own practical experience, distortions due to small loop sizes rather decrease when the ground is more conductive.

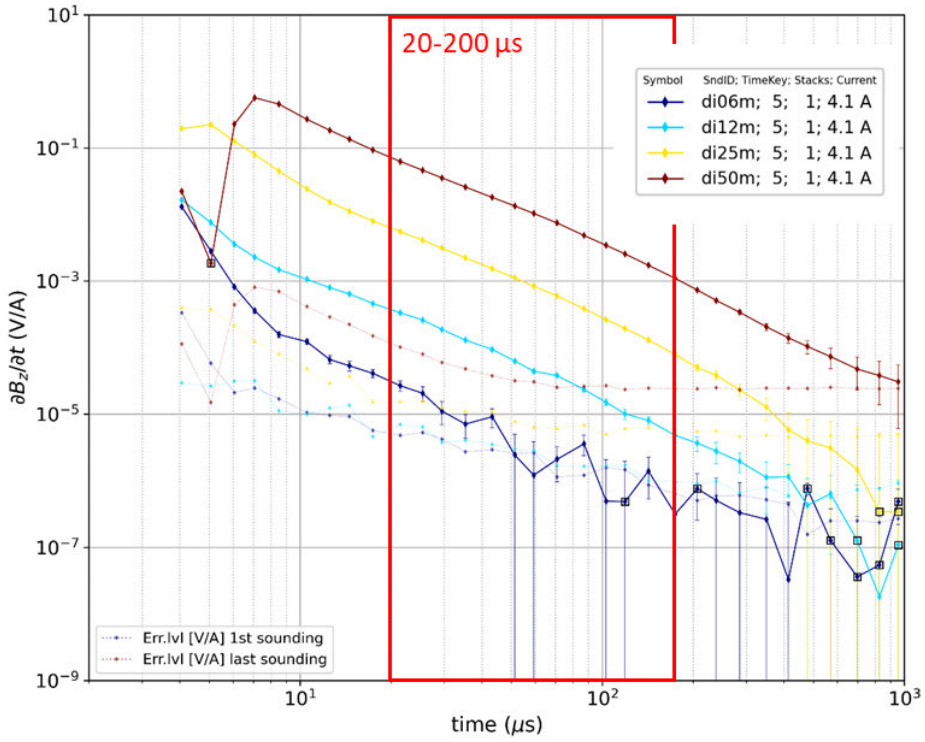

Figure R2.1. *Impulse response of a single-loop configuration using a TEMfast device at a side with an average resistivity of 120 Ωm across the uppermost 50 m (Donau Island, Vienna, Austria). The solid lines show the impulse responses for square loops with side lengths of 6 m (dark blue), 12 m (light blue), 25 m (yellow), and 50 m (brown). The dotted lines show the corresponding error levels (determined as the standard deviations of the repeated measurements). The red rectangle highlights the time window between 20 – 200 µs, to which the transients of our study at the Mexican lakes were truncated uniformly.*

M: In the discussion section, we added a short comment on possible distortions due to small loop configurations and shortly discuss the (probable) absence of such adverse effects in our data set. The exemplary data and inversion model responses for TEM measurement in the new appendix furthermore enable the reader to follow this discussion and to visually assess the data quality.

We have not included the above test measurements with different loop sizes in order to avoid overloading the manuscript.

• A conductor is indicated below the limestone towards the east in Fig. 7a. Please discuss this feature if it can be related to any geology such as fracture zones or if this is an artifact (probably related to distorted late time transient data). A slightly similar feature is also seen in Fig. 9 towards the south.

A: Unfortunately, both conducting features (old Figures 7a and 9a) are located at the very ends of the TEM lines, which are not covered by the collocated TDIP profiles. In addition, geological reference data, such as detailed maps or even drillings, are not available for these depths. Thus, we do not have any control on the nature of these features, i.e., we cannot decide whether they reflect a geological feature (e.g., a fracture zone or a more conductive claystone unit) or arise from distorted late time data.

M: We included a discussion of this issue into the revised version of the manuscript.

• Does the ZOND software actually invert for coincident loop or for a central loop receiver? For very early times the central loop transients differ from coincident loop data.

A: In order to be sure, we have checked this detail with the author of the code (Alex Kaminsky, zondgeo@gmail.com). His response can be summarized as follows: The software ZondTEM1d supports any arbitrary shaped loops, the vertices of which can be defined independently. The response is calculated as the integral along the transmitter loop path, i.e., the transmitter loop is implemented as a set of directed electrical dipoles. The same applied to the receiver loop, where the response (Bz) is integrated over the exact area of the receiver area.

M: We briefly mention this detail in the revised methods section.

• The TEM data might be effected by 2D effects especially considering rather steep slope angles towards the edges. possibly include some discussion such as “multidimensional effects in TEM data were not considered as the TEM survey lines were not along strong bathymetry or steep slopes”.

A: We are aware of the possible problems of multidimensionality can cause in the 1D interpretation of TEM soundings on lakes with steep bathymetry gradients (see, e.g., the extensive discussion of this issue provided by Mollidor et al., 2013). As you mention, the variation of the bathymetry along the lines shown here is relatively slight, which implies that this type of problem will probably not be of great relevance here. The assumption of onedimensionality might be more problematic at sounding sites located close to the lake shore.

M: We included a corresponding note in the methods section and come back to this topic in the discussion of the two profiles with TEM results to confirm that the bathymetry only varies softly along both lines and the assumption of one dimensionality is suitable, here.

• P315 - Obviously the p-wave velocity is less than expected. Can you elaborate why a lower vp < 2000 m/s was observed in the SRT measurements.

A: Possibly a misunderstanding? The depth of investigation of this SRT line (approx. 40 m below the water table of March 2018) is less than the depth of the surface of the limestone bedrock inferred from the TDIP resistivity section (> 40 m). Thus, the p-wave velocity at the lower limit of the SRT image is not lower than expected but lower than the typical p-wave velocity in the limestone unit.

M: We substitute the formulation “expected for limestone bedrock” by “typical for the limestone bedrock” to prevent this misunderstanding to happen.

• P350 - I suggest to include a table that summarizes the specifications of each method such as resolved physical parameter, DOI, pro/con of each method. Such a table would also summarize the used methods a bit and emphasize the integrative approach.

M: We liked this idea very much and included the new Table 2 into the revised manuscript, which summarizes the characteristic, the scope and limitations of all 4 field methods, i.e. SBP, TEM, TDIP, SRT.

• P-365 - For TEM a water-depth of 20 m depending on the water conductivity is not necessarily a limitation. Please correct this statement.

A: We fully agree: Due to the maximum water level reduction of about 20 m (from March 2018 to October 2019), we were only able to collect additional data on the dry lake floor at locations with less than 20 m of water column during our water-borne measurement campaign. This is the water depth down to which we were able to have a direct comparison of water-borne TEM data and

terrestrial TDIP data. Of course, this does not imply that the system does not also work in deeper water.

M: We added the following sentence to prevent possible misunderstandings: “Furthermore, there is no reason to assume that the system should not work as well in even deeper (>20 m) water depending on the water conductivity.”

• For all interpretation a smoothness constraint inversion is used. Do you expect a smooth transition from the sedimentary layers to the limestone. In this respect, is a smoothness constraint inversion appropriate to image the geological situation here?

A: Actually, we have been thinking about including seismic contacts (from SBP images) as a-priori information (geometric constraints) into the TDIP and SRT inversion process. However, we decided not to further pursue this approach as we consider it more conclusive to have various methods confirming similar structures without “forcing” geometries to coincide by using constraints in the inversions.

While we do not see any real alternative to a smooth inversion of our 2D data sets (i.e., TDIP and SRT), we do agree that it is not as straight forward to only discuss the results of a smoothness constrained approach for the TEM inversion. Here, the decision to only show the smooth models was motivated by facilitating the intended comparison with the (smooth) TDIP resistivity images.

In addition, there is no simple answer to the question whether we expect a sharp resistivity contrasts between the main lithological units, i.e.., sediment cover and limestone, or not. As our interpretation of the Metzabok data suggests, within the mixed layer (sediment and limestone debris/heavily fractured limestone) there might well be a rather smooth transition as a result of a continuously increasing volume content of limestone with depth. The same is true for the contacts between the different sedimentary units (fine-grained lake sediments/sandy delta deposits), which we expect to be rather gradual, too.

M: We included layered models into the visualization of the TEM resistivity models (i.e., Fig. 7a and 10a of the revised manuscript). We also include a short discussion of these two inversion approaches into the revised discussion section.

• As water-borne TEM studies are still quite rare, I miss some references to recent water borne TEM studies. For example, we recently applied boat-towed TEM to image a hydrothermal target on the Azores. In this study we gathered around 600 soundings using the TEM system (initially developed by Mollidor et al.) in a continuous mode. There are also other very recent studies. These can be included as references, if the authors find them suitable:

- Yogeshwar, P., Küpper, M., Tezkan, B., Rath, V., Kiyan, D., Byrdina, S., ... & Viveiros, F. (2020). Innovative boat-towed transient electromagnetics Investigation of the Furnas volcanic lake hydrothermal system, Azores. Geophysics, 85(2), E41-E56.

- Lane Jr, J. W., Briggs, M. A., Maurya, P. K., White, E. A., Pedersen, J. B., Auken, E., ... & Adams, R. (2020). Characterizing the diverse hydrogeology underlying rivers and estuaries using new floating transient electromagnetic methodology. Science of The Total Environment, 140074.

A: Thanks a lot for the hint! We missed these very recent studies. They are more than relevant.

M: We updated the state-of-the-art part on boat-towed TEM devices accordingly and included these additional references.

3. Technical corrections

The MS is very well written and the language is very good. All figures are well prepared with well readable fonts. Therefore, I only have a few technical corrections:

• P70 - the term reference data is misleading. I do not see that the data is actually used as reference data. Better - “additional/complementary data for comparison with the water borne data”

M: We replaced the term “reference data” by “additional data”.

• Please check that all abbreviations are defined, e.g. ERT etc.

A: We have checked the abbreviations. Besides the undefined abbreviation ERT (line 77 and in the caption of Figure 6), we have not found any additional problems with undefined abbreviations.

M: We replaced the term “ERT results” in line 77 by “TDIP resistivity results” and the term “ERT/IP data” in the caption of Figure 6 by “TDIP resistivity and phase data”.

• P140 - explain or remove the skip parameters (skip-1 skip-2 etc.)

M: We removed the skip parameters specified between the brackets.

~~Water- and land-borne geophysical surveys before and after the sudden water-level decrease of two large karst lakes in southern Mexico~~Integrated land and water-borne geophysical surveys shed light on the sudden drying of large karst lakes in southern Mexico

Matthias Bücker[1,2], Adrián Flores Orozco[2], Jakob Gallistl[2], Matthias Steiner[2], Lukas Aigner[2], Johannes Hoppenbrock[1], Ruth Glebe[1], Wendy Morales Barrera[3], Carlos Pita de la Paz[4], Emilio García García[4], José Alberto Razo Pérez[4], Johannes Buckel[1], Andreas Hördt[1], Antje Schwalb[5], Liseth Perez[3,5]

1Institute for Geophysics and Extraterrestrial Physics, TU Braunschweig, Braunschweig, 38106, Germany.
2Department of Geodesy and Geoinformation, Research Group Geophysics, TU Wien, 1040, Austria.
3Instituto de Geología, Universidad Nacional Autónoma de México, Mexico City, 04510, Mexico.
4Geotem Ingeniería S.A. de C.V., Mexico City, 14640, Mexico.
5Institute of Geosystems and Bioindication, TU Braunschweig, 38106, Germany.

Correspondence to: Matthias Bücker, (m.buecker@tu-braunschweig.de)

Abstract. Karst water resources play an important role in drinking water supply, but are highly vulnerable to even slight changes in climate. Thus, solid and spatially dense geological information is needed to model the response of karst hydrological systems to such changes. Additionally, environmental information archived in lake sediments can be used to understand past climate effects on karst water systems. In the present study, we carry out a multi-methodological geophysical survey to investigate the geological situation and sedimentary infill of ~~The present geophysical study was motivated by the need to determine suitable coring locations for paleolimnological studies in~~ two karst lakes (Metzabok and Tzibaná) of the Lacandon Forest in Chiapas, southern Mexico. Both lakes present large seasonal lake-level fluctuations and experienced an unusually sudden and strong lake-level decline in the first half of 2019, leaving Lake Metzabok (maximum depth ~25 m) completely dry and Lake Tzibaná (depth ~70 m) with a water level decreased by approx. 15 m. Before this event, ~~We used seismic and transient electromagnetic methods to map the sediment thickness below the lake floor. When lakes were filled~~during a lake-level high stand in March 2018, we collected water-borne seismic data with a sub-bottom profiler (SBP) and transient electromagnetic (TEM) data with a newly-developed floating single-loop configuration. In October 2019, after the sudden drainage event, ~~The latter aimed at assessing the TEM method as an alternative to seismic methods for the investigation of lake sediments and geology. After the first campaign, water levels of both studied lakes dropped dramatically by July 2019, leaving Lake Metzabok (maximum depth ~ 25 m) dry and Lake Tzibaná (~ 70 m) with a water level decreased by approx. 30 m. After the sudden drainage of the lakes,~~ we took advantage of this unique situation and ~~complemented water borne measurements by a survey~~ carried out complementary measurements directly on the exposed lake floor of Lakes Metzabok and Tzibaná ~~in October 2019, when lake levels were still low~~. During this second campaign, we collected time-domain induced polarization (TDIP)~~,~~ and seismic refraction tomography (SRT) data ~~on the desiccated bed of Lake Metzabok and some dry~~

parts of Lake Tzibaná. By comparing integrating the various multi-methodological data sets,, we (1) identify 5-6 m thick, likely undisturbed sediment sequences on the bottom of both lakes, which are suitable for future paleoenvironmental drilling campaigns, (2) develop a comprehensive geological model implying a strong interconnectivity between surface water and karst aquifer, and (3) evaluate the potential of the applied geophysical approach for the reconnaissance of the geological situation of karst lakes. This methodological evaluation reveals that under the given circumstances, find that (i) SBP and TDIP phase images consistently resolve the thickness of the fine-grained lacustrine sediments covering the lake floor, (ii) TEM and TDIP resistivity images consistently detect the upper limit of the limestone bedrock and the geometry of fluvial deposits of a river delta, and (iii) TDIP and SRT images suggest the existence of a layer that separates the lacustrine sediments from the limestone bedrock and consists of collapse debris mixed with lacustrine sediments. While oOur results do not imply that resistivity-based methods could generally replace seismic reflection surveys for lake-bottom reconnaissance, they clearly show that that the combination of seismic methods, which are most widely used for lake-bottom reconnaissance, with resistivity-based methods such as TEM and TDIP can significantly improve the interpretation surveys can provide important complementary information andby resolvinge additional geological units or bedrock heterogeneities, which are not visible from seismic data. Only the use of complementary methods provides sufficient information to develop comprehensive geological models of such complex karst environments

The latter aimed at assessing the TEM method as an alternative to seismic methods for the investigation of lake sediments and geology.

1 Introduction

About 7–12% of the world's continental area is covered by karst (e.g., Hartmann et al., 2014) and up to one quarter of the earth's population at least partially depends on drinking water from karst systems (e.g., Ford and Williams, 2007). Even though continued population growth and industrialization put pressure on these important resources in terms of both water quantity and quality, the response of karst systems to expected future climate change is still not well understood (Hartmann et al., 2014). Groundwater models offer one opportunity to estimate future changes in water availability, but heavily depend on reliable and spatially dense geological information. Where direct geological information, e.g., from drillings, is not dense enough or not available at all, geophysical methods can be used to provide quasi-continuous indirect information on the subsurface geology in karst areas (Bechtel et al., 2007).

Another possibility to understand climatic effects on karst water systems relies on the analysis of paleoenvironmental records (e.g., Medina-Elizalde and Rohling, 2012; Vázquez-Molina et al., 2016). In particular, Ll ake sediments are important archives of freshwater and terrestrial environmental information and and in particular sediment cores can be used to reconstruct past climate and ecological changes in the lakes (Cohen, 2003; Schindler, 2009; Pérez et al., 2020). Thus, paleoenvironmental studies give insight into the local links between climate variations and the availability (and quality) in lakes and the connected karst aquifer system. The northern neotropical region hosts a large number of lakes of different origins (karst, volcanic, maar,

~~tectonic) (Pérez et al., 2011; Sigala et al., 2017). Recent studies have highlighted the great potential of sedimentary sequences from lakes in Mexico and Guatemala as continuous paleoenvironmental and paleoclimatic records during the late Quaternary (Díaz et al., 2017; Lozano et al, 2017; Cohuo et al., 2018).~~ To identify suitable drilling locations providing continuous paleoenvironmental records at a high temporal resolution, knowledge about sediment thickness and composition, depth to bedrock, and possible heterogeneities within the lake sediments is needed (Last and Smol, 2002).

Geophysical methods can efficiently provide such information from the local scale up to the lake-basin scale and can (principally) be employed on both land and water.

Due to the usually sharp contrast between seismic velocities of sediment layers and the underlying bedrock, (reflection-) seismic methods are often given priority over other geophysical methods for lake-bottom reconnaissance (Scholz, 2002). In particular, low-frequency echo sounders (e.g., Dondurur, 2018), also referred to as sub-bottom profilers (SBP), allow to quickly map sediment deposits of several tens of meters based on single-channel seismic data. Nevertheless, electrical-resistivity ~~data~~images provided by electrical resistivity tomography (e.g., Binley and Kemna, 2005) or electromagnetic soundings (e.g., Kaufman et al., 2014) ~~can~~ complement the mostly geometrical information obtained from reflection-seismic or sub-bottom profiling measurements (Butler, 2009). Under certain conditions such as high lake-bed reflectivity and/or low reflectivity of targeted boundaries, seismic methods may, however, provide insufficient results and therefore alternative methods are needed.

Recent studies using direct-current (DC) electrical resistivity for water-borne investigations on freshwater bodies include surveys with floating (e.g., Befus et al., 2012; Orlando, 2013; Colombero et al., 2014) or underwater electrode chains (e.g., Toran et al., 2015) and provide evidence for the potential of this method for shallow-water applications. Electrical resistivity can also be assessed by electromagnetic methods, which, compared to DC resistivity measurements, offer a more compact experimental layout. Electromagnetic surveys are often carried out as transient electromagnetic (TEM) soundings with floating magnetic sources and receivers. Hatch et al. (2010), for example, used an in-loop configuration with a ~7.5 m x 7.5 m transmitter and a ~2.5 m x 2.5 m receiver to map river bed salinization in an Australian river with an average water depth of 5-10 m. Mollidor et al. (2013) used a similar but slightly larger setup (~18 m x 18 m transmitter, ~6 m x 6 m receiver) to map a thick conductive sediment layer below the bottom of a 20-m deep maar lake in Germany. More recently, -Yogeshwar et al. (2020) used the system developed by Mollidor et al. to image a volcanic lake hydrothermal system on the Azores; whereas Lane et al. (2020) introduced a compact floating TEM system, designed for the rapid electrical mapping of the subsurface of rivers and estuaries. Some older relevant case studies with shallow-water applications of both techniques, DC resistivity and electromagnetic soundings, were reviewed by Butler (2009).

In a previous study, we successfully used geoelectrical and electromagnetic methods to investigate the sedimentary infill of two desiccated lakes in a volcanic area (Bücker et al., 2017; Lozano-García et al., 2017). To extend our investigations, ~~Here~~in this study, we evaluate~~add a systematic field study that assesses~~ the potential of ~~water~~ land and water--borne resistivity-imaging~~based~~ methods to complement seismic methods for the investigation of ~~water filled~~ karst lakes in the Lacandon Forest, southern Mexico. Recent biological and abiotic studies have highlighted the great potential of sedimentary sequences from the lakes of this remote area as continuous paleoenvironmental and paleoclimatic records during the late Quaternary (e.g., Díaz et

al., 2017; Echeverría-Galindo et al., 2019; Charqueño-Celis et al., 2020). In this study, we focus on Lakes Metzabok and Tzibaná, two of the largest lakes of the Lacandon Forest, which experienced a sudden and catastrophic lake-level drop in the first half of 2019. While large seasonal lake-level variations are part of the nature of both lakes, it remains unclear whether such particular events as the one observed in 2019, which left Lake Metzabok completely dry, are also recurrent with a frequency of several decades or rather linked to recent climate change. To better understand possible draining mechanisms and their triggers, besides further paleoenvironmental investigations, a comprehensive geological picture of the lakes´ geological situation is essential.

In 2018, roughly one year before the drainage event and . ~~The basic assumption behind this approach is that a (sufficiently thick) layer of fine-grained lakebed sediments would be more conductive than the underlying bedrock and the water column and thus detectable by resistivity-based methods. Because applications of transient electromagnetic (TEM) soundings on lakes are still rare, in this study, we are particularly interested in the evaluation of such water-borne measurements.~~

~~W~~when the lakes were filled, we collected seismic data with a SBP and carried out TEM soundings to assess the electrical resistivity of the lake bottom and obtain information on the thickness of the sedimentary infill. ~~As we used floating experimental setups for both methods, device and targeted sediment layer on the lake bottom were often separated by a water column of 20 m and more, with the corresponding limiting effect on the resolution of the sediment thickness estimates.~~ The sudden ~~and unexpected~~ drainage of the investigated ~~karst~~ lakes in 2019~~, which occurred only a few months after the water-borne survey~~, provided us with the unique opportunity to collect ~~reference~~ additional data directly on the dry lake bed. Seismic ~~reference~~ data was then recollected with a seismic refraction tomographic (SRT) setup in order to provide information on both refractor geometry and seismic velocities of the different geophysical units. Additional ~~E~~electrical imaging ~~reference~~ data was measured with the time-domain induced polarization (TDIP) method, which has fewer limitations regarding the detectability of thin near-surface layers and heterogeneities than the transient electromagnetic method. Furthermore, the polarization properties of the subsurface materials assessed by TDIP measurements provide additional information and can improve the interpretation of TEM and TDIP resistivity ~~ERT~~ results.

Based on the above considerations, our study has three main objectives: (1) Identify suitable drilling locations to obtain undisturbed and far-reaching sedimentary sequences for paleoenvironmental reconstructs, (2) provide basic knowledge on the geological situation of the studied lakes (sediment cover, limestone bedrock and possible connectivity with the karst aquifer), and (3) develop and apply a multi-methodological geophysical approach with a special focus on the ~~Because applications~~evaluation ~~–~~of the potential of water-borne ~~transient electromagnetic (~~TEM~~)~~ soundings for lake-bottom reconnaissance~~s on lakes are still rare, in this study, we are particularly interested in the evaluation of such water-borne measurements.~~

~~The basic assumption behind this approach is that a (sufficiently thick) layer of fine-grained lakebed sediments would be more conductive than the underlying bedrock and the water column and thus detectable by resistivity-based methods.~~

2 Study area

The study area is located in the Lacandon Forest (16°–17.5° N; 90.5°–92° W; 500–1500 m.a.s.l.), which occupies the north-eastern part of the State of Chiapas, Mexico. The region belongs to the Chiapas fold belt with its WNW-trending folds and thrusts (Fig. 1), which mainly developed in massive cretaceous limestone (García-Gil and Lugo Hupb, 1992). The orogeny of the Chiapas fold belt is related to the collision of the Tehuantepec Transform/Ridge on the Cocos plate with the Middle America Trench during the Middle Miocene (Mandujano-Velazquez and Keppie, 2009). The resulting anticlines and synclines dominate the topography in the study area forming long WNW-directed valleys and mountain ranges. The tectonically fractured limestone geology, in conjunction with the humid subtropical climate, favour an intensive karstification (García-Gil and Lugo Hupb, 1992). In the valleys, lakes formed by bedrock dissolution, such as dolines (or sinkholes), uvalas (formed by two or more dolines) and poljes (larger karst depressions), are mostly aligned in the main fold direction.

The lake system of Metzabok (17°6'30"–17° 8'30" N, 91°36'30"– 91°38'50" W, ~550 m a.s.l.) consists of 21 lakes of different sizes, the majority of which are interconnected when water levels are high (Lozada Toledo, 2013). The two largest lakes of the system are Lake Tzibaná (area 1.24 km²; max. depth 70 m) and Lake Metzabok (0.83 km²; 25 m) (see Fig. 1). The river Nahá is the principal superficial tributary connecting the lake system of Metzabok with the one of Nahá (~830 m a.s.l.); a superficial outlet of the lake system does not exist. Although the (additional) water supply and discharge through the underlying karst system is unknown, fast lake-level changes indicate substantial groundwater-surface water connections ~~a dominant role of subsurface hydrology~~. Usually, seasonal lake-level changes amount to ~10 m and can be traced back to prehispanic times (Lozada Toledo, 2013). Between March and August 2019 an extreme lake-level drop occurred that left Lake Metzabok completely dry and decreased the water level of Lake Tzibaná by ~~–~~13~~0~~5 m.

3 Data acquisition and processing

With the ~~overall~~ primary goal of mapping sediment thicknesses below the lake floor of various lakes of the karst lake systems of Metzabok and Nahá, we carried out a first geophysical campaign employing seismic (SBP) and TEM methods, when lake levels were maximum in March 2018 (Fig. 2a). Immediately after the dramatic lake-level decline, we revisited the study site in October 2019 to collect refraction seismic tomography (SRT) data and perform TDIP measurements directly on the dry lake bottom (Fig. 2a, b).

3.1 Electrical resistivity measurements in the laboratory

In October 2019, a total of six surface sediment samples (top 10 cm) and two water samples were collected at different locations for laboratory analyses (see sampling locations in Fig. 2a, b). On the dry lake bottom, sediment samples were collected using a small spade, whereas an Ekman grab sampler was used to retrieve sediment samples from water-covered areas. Sediment samples were stored in sealed plastic bags in order to prevent the loss of moisture; water samples were stored in plastic bottles. All samples were kept cool during transport and storage in order to prevent an increased degradation of organic matter. The

electrical conductivity of the water samples (at 20°C) was measured with a laboratory probe. The frequency-dependent complex electrical resistivity of the samples was measured using a Chameleon I measuring device (Radic Research) in the frequency range from 1 mHz to 240 kHz. To this end, the unconsolidated sediments were filled into four-point measuring cells with non-polarizing potential electrodes as used by Kruschwitz (2007) and Bairlein et al. (2014). Prior to and during the measurement, the measuring cell was stored in a climate chamber to keep the sample at a constant temperature of 20°C. Measurements were repeated over a period of 4 to 5 days after filling the cell and inserting it into the climate chamber in order to assure equilibrium conditions in the sample. Measurements on relatively dry samples (MET19-A and TSI19-A) resulted in comparably high phase values. These samples were removed from the measuring cell, saturated with water of the corresponding lake (using one of the two water samples), and filled again into the measuring cell. This procedure led to more consistent phase measurements compared to the other samples.

3.2 Collection of sub-bottom profiler (SBP) lines

Low-frequency echo-sounders, often referred to as sub-bottom profilers (SBP), are single channel seismic reflection systems, which are used to obtain bathymetric profiles and provide a high-resolution stratigraphic display of the uppermost sediments (e.g., Dondurur, 2018). In March 2018, SBP lines were collected with the 10-kHz transducer StrataBox HD (SyQwest), which has an output power of 300 W, mounted on a motor boat. Data was recorded with a record length of 200 ms and a 1024 Hz sampling frequency. The SBP device was mounted mid-ships in a side mount configuration, with the transducer positioned at 0.4 m below the water surface. Prior to each survey, the acoustic wave velocity profiles of the water columns of the two studied lakes were measured with a Digibar S (Odom Hydrographic). SBP lines were laid out in a regular NS- and EW-oriented grid with separations of 100 m and 300 m, respectively (see Fig. 1). Navigation data was measured with a differential GPS and stored along with the SBP data.

During processing, the SBP acoustic traces were read in using code provided by Kozola (2020) and visualized using a Matlab script available with this manuscript. The average value~~s~~ of the acoustic wave velocity of the water column~~s~~ (1486.6 m/s for both lakes) were used to convert the two-way travel time of the acoustic pulse into a depth scale for the seismic profiles.

3.3 Transient electromagnetic (TEM) soundings

Transient electromagnetic (TEM) soundings were carried out from the water surface using a single-loop configuration in March 2018. The loop with a diameter of 22.9 m (surface area: ~412 m²) consisted of a single, insulated copper wire attached to a floating ring made of twenty-four 1-inch PVC tubes. The ring was towed by an inflatable boat equipped with an electric motor, which was only turned on for navigation between sounding sites. During the measurements, the loop was separated by 5 m from the inflatable boat. Depending on the specific wind conditions, the unanchored system slowly drifted during the measurements resulting in maximum displacements of approximately two times the loop diameter (i.e., ~40 m). ~~, where it was connected to the measuring device, a TEM FAST48 (manufactured by Applied Electromagnetic Research). During the measurements, the loop was separated by 5 m from the inflatable boat.~~ Due to the comparably low measurement velocity (ca.

3 min per sounding) and the poor maneuverability of the experimental setup, TEM data was acquired along a limited number of irregularly distributed lines of interest (Fig. 2a).

A simple echo-sounder (Garmin Fishfinder series) was used to measure the water depth at each sounding site. ~~For the acquisition of TEM sounding data, we used a~~A TEM-FAST48 (manufactured by Applied Electromagnetic Research) was used for the acquisition of TEM sounding data.~~transmitter current of 1 A , and 3328 t~~Transients were recorded using ~~stacked at each sounding site with~~a transmitter current of 1 A and ~~in~~ 32 time gates between 3.6 µs and 1024 µs after current shut-off. For this transient length, the measuring device records 64 transients, which are analogously averaged by the hardware. For one sounding measurement, this basic measuring cycle is repeated $n \times 13$ times. For $n = 4$, which we used for our measurements, this results in 52 repetitions of the basic cycle and a total of 3328 effective stacks, which are used to compute the impulse response by digital averaging and to determine the measurement error as the standard error of the mean (SEM). For times around 200 µs (the latest time gates used for the inversion), the SEM is $\lesssim 5 \cdot 10^{-9}$ V/Am². For exemplary TEM data and errors, see Figure A1 of the appendix.~~Due to the comparably low measurement velocity (ca. 3 min per sounding) and the poor maneuverability of the experimental setup, TEM data was acquired along a limited number of irregularly distributed lines of interest (Fig. 2a).~~

During the processing, all transients were truncated to times from 21.4 and 174.5 µs ~~20 to 200 µs~~ and inverted using the software ZondTEM1d (A. Kaminsky, personal communication). A conventional 1D smoothness-constrained modelling approach was used to obtain a one-dimensional multilayer model (20 layers) for each sounding ~~site~~ position separately. ZondTEM1d supports arbitrarily shaped loops, whose vertices can be defined independently for transmitter and receiver to ensure the correct interpretation of the coincident-loop data. The same software was also used to adjust layered models (5 layers). In both cases (smooth and layered model), ~~T~~the water depth measured with the echo-sounder was used as a-priori information by fixing the thickness of the first layer to this value. The electrical resistivity of the water layer was fixed to 25 Ωm. This value was manually adjusted to provide a good overall fit for all soundings. Especially for sites with shallow water depths and a resistive lake bed (i.e., bedrock not covered by conductive sediments), constraining the resistivity of the water layer significantly improved the imaging results. Multidimensional effects, as investigated in detail by Mollindor et al. (2013) for TEM data from a lake with steep bathymetric slopes, were not considered in the interpretation as the bathymetric variation along our survey lines was relatively gentle. Following the approach by Yogeshwar et al. (2020), which is based on the one by Spies (1989), we estimate the depth of investigation (DOI) of our TEM soundings based on transmitter area and current, average subsurface resistivity (of the smooth models), and late-time induced voltage.

3.4 Time-domain induced polarization (TDIP)

Time-domain induced polarization (TDIP) data was acquired with a SyscalPro Switch 48 device (IRIS Instruments) using 48 stainless-steel electrodes separated by 5 m or 10 m depending on the target. The soft and wet mud on the exposed lakebed provided a good contact between electrodes and ground. Where TDIP profiles crossed limestone outcrops, electrodes were inserted into sediment-filled fractures in order to keep contact resistances as low as possible. Measurements were carried out

with injection currents between 0.5 A and 1 A, one single stack and a 50% duty cycle with 500 ms pulse length (i.e., duration of off time is also 500 ms). After an initial delay of 20 ms after current shut off, the voltage decay was sampled in 20 time windows with a constant length of 20 ms. We used a dipole-dipole configuration combining short dipole lengths of one electrode spacing ~~(skip 0)~~ for superficial measurements with longer dipole lengths of two and four times the electrode spacing ~~(skip 1 and skip 3)~~ for moderate and large depths, respectively. To prevent loss of data quality due to remnant electrode polarization (e.g., Dahlin et al., 2002), the measurement protocol avoids potential readings using electrodes that had been used as current electrodes before (Flores Orozco et al., 2012; 2018a) ~~(Dahlin et al., 2002)~~. TDIP lines of varying length were laid out along (and parallel to) selected 2018 SBP and TEM lines on both lakes (Fig. 2a, b). In order to cover the full length of the north-south running SBP line L4 NS, TDIP lines MET19-1 and MET19-2 were carried out as a roll-along profile with an electrode spacing of 10 m and an overlap of 12 electrodes.

During the processing, we removed erroneous measurements defined as those associated with negative apparent resistivity and/or integral chargeability readings (Flores Orozco et al., 2018b). After the removal of erroneous measurements, raw-data pseudo sections were inspected and additional outliers were defined as those readings with integral chargeability values above ~~6~~ 8 mV/V. Based on an exemplary data set, this processing approach is further discussed the appendix. Integral chargeability values were then linearly converted to frequency-domain phase shifts assuming a constant phase angle response (i.e., no frequency dependence) following the approach outlined by Van Voorhis et al. (1973) and implemented by Kemna et al. (1999). Finally, 2D complex-resistivity sections were ~~then~~ reconstructed from the filtered data using the smoothness-constrained least-squares algorithm CRTomo (Kemna, 2000). 2D sections are only visualized down to an estimated depth of investigation by blanking model cells with cumulated sensitivity values two orders of magnitude smaller than the maximum cumulated sensitivity (i.e., the sum of absolute, data-error weighted, sensitivities of all considered measurements; e.g., Weigand et al., 2017).

3.5 Seismic refraction tomography (SRT)

Seismic-refraction tomography (SRT) data was acquired with the 24-channel seismograph Geode (Geometrics) and twenty-four 28-Hz geophones installed along a line at 5 m spacing in October 2019. To generate the seismic signal, a 7.5 kg sledgehammer hitting a steel plate was used at 25 shot points between the geophone positions as well as at distances of 2.5 m from the first and last geophone, respectively. At each shot point, five shots were stacked to improve the signal-to-noise ratio. Due to the limited length (115 m between the first and the last geophone) and investigation depth, SRT data was only collected in the central parts of selected TDIP profiles (Fig. 2a, b).

During the processing, we applied a 120 Hz low pass filter on the seismic traces to remove high frequency noise and allow for a more accurate picking of first break travel times.

~~Based on the first arrival travel times, a~~A tomographic inversion scheme then determines the two-dimensional velocity structure below the SRT profile based on the first-arrival travel times (e.g., White, 1989). For the filtering of the seismic traces and picking of the first arrivals, we used a Python toolbox developed at the TU-Wien. The observed travel times were ~~then~~

inverted with the pyGIMLi framework (Rücker et al., 2017) following a smoothness-constrained scheme. Based on the ray paths computed for the resolved velocity model (e.g., Ronczka et al., 2017), we also determine the so-called ray coverage, which permits to illustrate the depth of investigation by blanking models cells that are not covered by any ray. ~~Due to the unconsolidated, muddy ground encountered on the lake floor, the signal-to-noise (S/N) ratio of the SRT data was challenging and lead to a low picking percentage, especially at larger offsets (distance between shot point and geophone location).~~

4 Results and interpretation

4.1 Laboratory measurements – electrical properties of sediment and water samples

The complex-resistivity measurements on the six sediment samples carried out in the laboratory (Figure 3) show that most resistivity values vary within a relatively narrow range between 10 and 15 Ωm. Only the resistivity of one sample (TSI19-A) from the river delta in Lake Tzibaná reached values between 18 and 20 Ωm. Figure 3b shows that phase values (here $-\varphi$) in the frequency range from 1 to 10 Hz, which is mainly tested by our TDIP measurements, are roughly comprised between 0.5 and 4 mrad. Again, the only exception is sample TSI19-A with phase values of up to 6 mrad in the relevant frequency range. We attribute the atypical behavior of the sample TSI19-A to its fluvial nature (coarse grains and high organic content), while the remaining samples are clearly lacustrine (fine grains and lower organic content). The elevated phase values at high (>1 kHz) frequencies, which can be observed for all six samples, -are typical electromagnetic coupling effects (Pelton et al., 1978), but do not affect our TDIP measurements, due to the long initial delay before the sampling of the voltage decay starts.

The resistivity of the two water samples from the remaining water bodies used to improve the readings of two dry samples (MET19-A and TSI19-A) were 11.9 Ωm (Metzabok) and 26.8 Ωm (Tzibaná), respectively. They are significantly lower than the average water resistivity of ~34.5 Ωm reported by Rubio Sandoval (2019) for water samples collected from Lake Metzabok during high lake-level stands in 2016. This reduction of electrical resistivity (i.e., increase of conductivity) is probably due to the larger effect of evaporation on the salinity of small (and shallow) water bodies. Indeed, the remaining water body in Lake Metzabok was much smaller (~50 m²) than the one in Lake Tzibaná (~5000 m²).

The average resistivity of the sediment samples for the frequency range between 1 and 117 Hz (and excluding sample TSI19-A) is 12.25 Ωm, which is typical for saturated clayey sediments (e.g., Reynolds, 2011). Note that due to the contribution of surface conduction along the charged clay-mineral surfaces (Waxman and Smits, 1968), the bulk resistivity of the sediments is even lower than the average resistivity of the water (~25-35 Ωm ~~(~~ during high lake-level stands). In our case, this resistivity contrast between lake water and sediments by a factor of 2 to 3 is of particular relevance as it allows us, in principle, to detect the two materials as separate units. To our best knowledge, this is the first time that the phase spectra of fresh lake-bed sediments have been measured in the laboratory.

4.2 Field measurements on Lake Metzabok

In October 2019, Lake Metzabok (average depth 15 m) was completely dry, except for some residual ponds. Its sediment-covered bottom is mostly flat with steep walls (>50% slope) and some cliffs along the shore line (Fig. 4a). Only some drainage channels, steep limestone hillocks, and small ponds (Fig. 4a–d) eventually disrupt the smooth lake-bottom topography.

4.2.1 Profile 1 – SBP and TDIP results reveal three distinct geological units

The north-south oriented SBP line L4 NS on Profile 1 crosses various of these ~~topographic elevations~~limestone hollocks and depressions, which are well resolved by the first reflector in the seismogram (Fig. 4e). Within the depressions between the limestone outcrops, a second reflector can be resolved, the geometry of which shows a certain consistency with the surface of the limestone outcrops. This reflector~~,~~ can be interpreted as the lower limit of the sediment cover. The SBP data ~~clearly~~ shows that not only the elevations (outcrops) but also the depressions in the sediment cover are influenced by the topography of the underlying limestone: Both depressions, the drainage channel in the northern as well as the small pond in the southern part, are associated with local heights in the limestone surface. Based on the SBP images, the sediment thickness mostly varies between 5 and 7 m along Profile 1.

Below the surface of the limestone outcrops and the lower limit of the sediment cover, respectively, we observe zones of diffuse reflectivity. These might be related to the heavily fractured and dissolved limestone. Particularly in the flat areas, the sediment cover might also be underlain by blocks of collapsed limestone with sediment filling the spaces between blocks and debris. The lakes of the study area show all characteristics of karst lakes, which are expected to originate from collapsed karst cavities, and the collapse debris should still be present below the sediment cover.

The electrical images obtained from the co-located TDIP line (MET19-1 and 2) supports this interpretation: The resistivity image (Fig. 4f) shows a gross separation into two main units: The (i) sediments as well as the supposed limestone debris-sediment mixture stand out with low resistivity values between 10 and 20 Ωm, while the (ii) limestone outcrops and the deep part of the section are characterized by higher resistivity values of up to 300 Ωm. The phase image (Fig. 4f) also shows a separation into units with low and intermediate phase values. Here, a much thinner top layer (compared to the conducting layer in Fig. 4f) stands out with phase values between 0 and 5 mrad, while the limestone bedrock shows phase values >5 mrad. Due to the relatively low data cover after outlier-removal for large dipole separations, we do not interpret the phase values at depths >50 m.

For the sediment infill, both the resistivity values of 10-20 Ωm and the phase values below 5 mrad are in agreement with our laboratory measurements on the sediment samples of Lake Metzabok, corresponding to an average resistivity of ~12 Ωm and phase values (here $-\varphi$) < 4 mrad. In contrast, resistivity and phase values associated with the limestone bedrock are significantly higher than those of the fine-grained sediment cover. The intermediate layer, which we interpret as mixture of fine-grained sediments and the collapse debris, seems to inherit the low resistivity of the supposed clay-rich matrix, while the phase or polarization response is increased by the limestone debris.

4.2.2 Profile 2 – SRT measurements confirm the presence of three geological units identified in the TDIP images

The north-south oriented Profile 2 runs parallel to the last part of Profile 1 but shifted ~10 m East. It is centered at the small pond (Fig. 4d) and has a smaller electrode spacing (5 m instead of 10 m) to better resolve the sediment-limestone contact below the bottom of the pond. The electrical images (Fig. 5a, b) show the same characteristics as seen in the corresponding part of Profile 1. Due to the higher resolution, here, we observe an internal layering of the shallow conductive units with a less conductive (30-50 Ωm) top layer of ~10 m thickness and a more conductive (<20 Ωm) layer that extends down to 30 m in the northern and southern parts of the line. The separation into two units becomes ~~much~~ more obvious in~~from~~ the phase image, where the superficial layer is less polarizable (well below 4 mrad) than the deeper part. A few meters East of the centre of the profile, the resistive limestone bedrock crops out, which might explain the significantly increased resistivity (>100 Ωm) and phase values (>6 mrad) over the first 20 m of depth below this part of the profile.

The p-wave velocity structure in the SRT image (Fig. 5c) confirms the presence of these three units: The shallowest layer, corresponding with the sediment infill characterized by velocities between 200 and 1000 m/s, which is in agreement with values for unconsolidated fine-grained sediments reported in the literature (Uyanık, 2011). In the second layer, velocities increase to 1500-2000 m/s, and at depths between 15 and 20 m, a sudden increase to values >2500 m/s is observed. The p-wave velocities of the deepest unit agree with the lower limit of typical ranges for limestone (Reynolds, 2011), which can be explained by the high degree of fracturing and dissolution of the karst bedrock. The seismic velocities of the intermediate layer do not provide any additional information on its nature, but could well be explained by limestone debris or heavily fractured and dissolved limestone with sediment-filled open spaces.

4.2.3 Profile 3 – Comparison of SBP and TDIP corroborates low phase response of lake sediments

The comparison of the SBP line along the west-east directed Profile 3 with the corresponding electrical resistivity images (Fig. 6) confirms the interpretation of the electrical images: The step in the lower limit of the sediment layer around 490 m along the SBP profile, is also reflected in the resistivity structure and it is clearly resolved in the phase image. Again, the conductive unit extends far below the SBP reflector, in particular between 440-490 m along the profile. ~~As w~~We interpret this reflector as the contact between pure sediments and the mixed sediment-collapse debris. Thus, ~~, this means that~~ the mixed layer has a lower resistivity than the superficial fine-grained sediment layer. Along this profile, both sediment-bearing layers are characterized by low phase values. The sediment-covered limestone bedrock between 440 and 530 m is characterized by high phase values, while phase values decrease as this unit approaches the surface and crops out at the end of the profile. The low phase values of the limestone outcrop do not fit the previously stated general characteristics of this unit but might be related to variations in composition and/or degree of fracturing of the limestone bedrock.

4.2.4 Profile 4 – Water-borne TEM and terrestrial TDIP measurements reveal consistent resistivity models

Fig. 7a shows the electrical resistivity image reconstructed from 12 TEM soundings along the profile crossing Lake Metzabok from W~~Northw~~est to ~~Southe~~East. Both, smooth and layered models, recover ~~A~~a conductive layer of varying thickness below the lake floor indicating~~es~~ the presence of fine-grained sediment infill across the entire basin. This layer only disappears close to the shoreline (i.e., towards the eastern end of the profile), where the resistive limestone bedrock is in direct contact with the water body. According to the layered model, the resistive bedrock itself is encountered at depths of approx. 15-20 m below the lake bed and only disappears below sounding MET10, where a possible fracture zone might be responsible for a lower resistivity at depth.

At both ends of the profile, and in particular at stations MET1 and MET2, a conductor is indicated below the resistive bedrock, this could also point to a more fractured bedrock or a lithological contact, e.g., with a shaly geological unit. However, in absence of complementary information, such as a detailed geological map or bore hole data, we can also not discard artefacts due to distorted late-time transient data. Especially close to the shoreline, where the lake bottom rises steeply, the TEM transients might additionally be affected by multidimensional effects (e.g., Mollidor et al., 2013), which are not taken into account by the chosen one-dimensional inverse modelling approach.

Due to the relatively high average resistivity of the subsurface along this profile, the depth of investigation (DOI) computed after Spies (1989) and Yogeshwar et al. (2020) is mostly larger than the 80 m shown here. Possibly due to the large resistivity and thickness of the limestone bedrock, no changes of the modelled resistivity have been observed at depths >80 m.

Between stations MET3 and MET7, the TEM image recovers a resistivity distribution similar to the one of co-located TDIP profile (Fig. 7b). Taking into account that the water-borne TEM survey was carried out with an average of 15 m water column, the consistency with the TDIP resistivity results from the lake bed clearly indicates a ~~high~~good quality and reliability of the obtained TEM imaging results.

As observed before, the phase image (Fig. 7c) shows a non-polarizable top layer, which at a depth of ~10 m is underlain by a unit with a higher polarization response (absolute phase values around 10 mrad and higher), corresponding with the debris-sediment unit. The SRT tomogram (Fig. 7d) shows a sharp increase in p-wave velocity at depths between 20 m (in the western part) and 30 m (in the eastern part). This southeast-dipping surface correlates with a similar structure in the TDIP resistivity model, which we again interpret as the contact with the limestone bedrock.

4.2.5 Geological interpretation of the geophysical survey on Lake Metzabok

The schematic sketch presented in Fig. 8a summarizes our geological interpretation of the geophysical profiles of Lake Metzabok and the observations made on the exposed bed of the drained lake. It rests on the assumption that the lakes in the study area are formed by the coalescence of a number of dolines that resulted from the collapse of karst cavities. The remains of the collapsed limestone are expected to have formed a debris layer covering the floor of the former caves. Subsequently,

the fluvial input of fine-grained lake sediments has first filled up the interspaces between the blocks and then buried the collapse remains, forming the two uppermost units observed below all profiles.

Table 1 summarises the physical properties of the main units of this geological interpretation. The electrical resistivity of the fine-grained sediments and the mixed collapse debris and sediment layer is comprised within a relatively narrow range. In the TEM and TDIP resistivity images, these two units may appear as one conductive unit (see red dotted lines in Fig. 8). It is not clear, why the addition of the more resistive lime stone debris should decrease the resistivity of the mixed unit compared to the pure fine-grained sediments. In terms of the phase values, the distinction between these units is clearer and the increase of the phase ~~values~~ response in the mixed layer is straightforward (because the limestone is more polarizable than the fine-grained sediments based on our field measurements). The clearest indication of the inner structure of the conductive unit comes from the collocated SBP sections, which show a clear seismic reflector at the corresponding depth. The limestone bedrock becomes detectable by its high p-wave velocity in the SRT images and its high resistivity (TEM and TDIP), while its phase response varies over a larger range and is, thus not as unambiguous. It is worth mentioning that wherever the fine-grained sediments are underlain by the collapse debris layer, the limestone bedrock does not appear as an additional reflector in the SBP sections.

4.3 Field measurements on ~~a river delta of~~ Lake Tzibaná

While the 2019 lake-level decrease left Lake Metzabok (max. depth 25 m) completely drained, the deeper Lake Tzibaná (max. depth 70 m) always preserved a water cover on at least 2/3 of its maximum surface area. The long N-S oriented SBP section in Figure 9 crossing the entire Lake Tzibaná (Profile 5) shows a similar lake-bottom architecture as the one derived for Lake Metzabok: Steep limestone walls along the shoreline and flat parts with the typical 3-layer structure consisting of fine-grained sediment cover, collapse debris, and limestone bedrock. Unlike in the case of Lake Metzabok, the flat parts of Lake Tzibaná are found at two different levels, which are separated from one another by a steep limestone cliff. Additionally, the southern part of the profile crosses ~~Besides the measurements in the completely drained Lake Metzabok, we also present data from one profile crossing~~ the delta of the Nahá river, where ~~in the southern part of Lake Tzibaná. The survey layout and satellite image in Fig. 2b show that the land-borne measurements (i.e., TDIP and SRT) along this profile only covered those parts of the river delta, which were dry during October 2019.~~

~~In contrast to the well-sorted and mainly fine-grained sediments (clay/silt) on the mostly flat bed of Lake Metzabok, here,~~ we expect a higher fraction of coarser material (sand/gravel) in the fluvial deposits in comparison to the well sorted sediments, mainly composed of clay and silt, ~~,~~ covering the flat parts of the lake bottom. In the SBP profile, these delta deposits stand out by a highly reflective lake bottom, which results in strong multiple reflections between lake bottom and water surface. Yet, such reflections inhibit the recovery of any information on the internal structure of the delta.

The TEM, TDIP, and SRT measurements carried out along Profile 6, which roughly covers the last 450 m of Profile 6 (see ~~The~~ survey layout ~~and satellite image~~ in Fig. 2b) fill in this missing information. ~~show that the land-borne measurements (i.e., TDIP and SRT) along this profile only covered those parts of the river delta, which were dry during October 2019.~~

~~Indeed, t~~The resistivity images of both TEM and TDIP measurements presented in Fig. 10~~9~~a, b consistently show three main units: (1) the resistive (>100 Ωm) limestone bedrock at depth, (2) a highly conductive (<10 Ωm) clay layer on top, and (3)~~, in particular between 200 and 400 m,~~ a layer of intermediate resistivity (~30-100 Ωm), in particular between 200 and 400 m, corresponding to the sand banks~~,~~ and ~~an~~ possible interbedded strata of clay, sand, and gravel associated with ~~, corresponding to~~ the ~~f~~delta~~luvial~~ deposits. As observed above along Profile 4, the resistivity model of TEM sounding TZI41 indicates a conducting unit below the resistive limestone bedrock, which could be related to a lithological contact, a fracture zone, distorted late-time data, or multidimensional effects. The low average resistivity below soundings TZI13-44 result in a significantly reduced depth of investigation (approx. 55-60 m). The lack of borehole data hinders a conclusive interpretation of this conductive anomaly at depth.

Probably due to the highly heterogeneous composition of the river delta, these deposits also show a heterogeneous distribution of phase values (Fig.~~ure 9~~10c). As observed before, the clay and limestone units below the fluvial deposits show low and high phase values, respectively. The relatively high phase values in the clay layer below the fluvial deposits are probably inversion artefacts caused by the relatively noisy TDIP data along this line.

The SRT image (Fig. ~~9~~10d) shows p-wave velocities as low as 100-200 m/s within the fluvial deposits, which are in agreement with literature values for partially saturated, unconsolidated sand (e.g., Barrière et al., 2012). P-wave velocities increase with depth across the thick (and probably compacted) clay layer. According to the electrical images, the surface of the bedrock lies below the lower limit of the SRT image. Accordingly, the highest velocities of <2000 m/s, seen in the SRT image, do not reach the high values (>2500 m/s) ~~expected~~ typical for limestone bedrock.

5. Discussion

5.1 Identification of suitable drilling locations

Our geophysical investigations delineate a 5-6 m thick and nearly undisturbed layer of fine-grained lacustrine sediments covering the flat parts of Lake Metzabok. Such layer is relevant for the conduction of paleolimnological perforations. Suitable drilling locations can be defined between 450 and 550 m, as well as between 600 and 700 m along Profile 1 (SBP profile in Fig. 4e). The large variation of the sediment thickness observed along Profile 3, which is perpendicular to Profile 1, underlines the need for a comprehensive pre-drilling investigation and an accurate positioning of the drilling equipment. The sediment layer between 100 and 200 m along Profile 5 represents a suitable drilling location for Lake Tzibaná (sediment thickness also 5-6 m). Although the deeper part of Lake Tzibaná is covered by sediments (between 400 and 600 m along Profile 5), too, sediment thicknesses in this part of the lake are smaller (only 3-4 m according to the SBP image) and drilling efforts would be more considerable, due to the larger water column at this location (approx. 30 m during water-level high stand in 2019).

With a thickness of >40 m according to our electrical imaging results, the sedimentary cover along Profile 5 of Lake Tzibaná (particularly between 250 and 400 m) is much thicker than the sediments covering the flat parts of both lakes. However, our

results also indicate that these sediments rather correspond to fluvial deposits of the river delta. In this depositional regime, we expect much higher rates of sedimentation and thus not necessarily an older paleoenvironmental record. Additionally, river deltas are much more dynamic systems, in which sediments are deposited, eroded, and redeposited repeatedly, which decreases the probability to obtain undistorted sediment records as encountered further off the shore.

5.2 Geological situation of the studied lakes and hydrogeological implications

Our field observations and geophysical imaging results also have important implications for the general understanding of the geological situation of the two studied karst lakes: Large areas of both lakes are covered by a layer of clayey sediments, which have a low hydraulic permeability. Thus, where it is thick enough (up to 5-6 m across large areas), this layer acts as a hydrological barrier between the lakes and the underlying karst. However, the remaining heavily fractured and uncovered limestone outcrops (e.g., Fig. 8b-d) effectively connect the lakes with the karst water system. This conclusion is underscored by the high velocity at which the two lakes drained practically simultaneously between February and July 2019. Accordingly, the sudden drainage of both lakes might be related to the same hydrogeological process.

While the interconnectivity between surface water and karst aquifer is well documented by field observations and further underpinned by the interpretation of our geophysical results (see Fig. 8), the specific cause(s) and mechanism(s) of the sudden drainage of Lakes Metzabok and Tzibaná remain unrevealed. The suddenness of the drainage, suggests that one or more previously clogged karst conduits were unplugged around these dates. Planned time-series analyses of hydrological and meteorological data in combination with paleoenvironmental studies on sediment cores will possibly provide more detailed insight into the mechanism and its triggers, and thus shed light on the question whether such catastrophic drainage events as the one observed during 2019 are linked to recent climate change or another geodynamic process.

5.3 Lessons learned from implementing a multi-methodological approach for lake-bottom reconnaissance

Only the combination of complementary methods employed in the present study allowed us to produce comprehensive geological models of the lake-bottom geology of the studied karst lakes. Table 2 summarizes the characteristics of the four field methods (SRT, TEM, TDIP, and SRT), the individual contributions of each method and their respective limitations identified in this study. In the following, we will discuss some important aspects of this overview in more detail.

5.3.1 Sub-bottom profiler reflection seismic method

For shallow-water applications, the compact and mobile experimental setup of the SBP technique offers clear advantages. Additionally, the high productivity and resolution in combination with the straight-forward interpretation of the SBP seismograms evidence that such reflection seismic methods are best suited for a first reconnaissance of the lake bottom. In comparison, water-borne TEM measurements are by far slower and more labour intensive (for both data collection and processing) and the resulting imaging results have a lower lateral resolution. In our study, the contact between fine-grained

clay sediments and the underlying mixed layer (collapse debris and sediment) was clearly visible from the SBP data, which permits a straight-forward estimation of sediment thicknesses along SBP survey lines. The contact or transition between mixed layer and limestone bedrock was also noticeable in the SBP images but the interpretation was not as clear as in the case of the first two layers and mainly built on the availability of complementary TEM and TDIP data. The main limitations of the SBP survey consist in the low depth of penetration of this method, which hardly reached 10 m below the lake bottom, and in the total lack of sub-bottom information as soon as the lakebed is covered by coarser sediments as observed in the deltaic region of Lake Tzibaná. Such "opaque seismic facies and high […] reflectivity" of fluvial sediments have been discussed before by Orlando (2013) for measurements on the river Tiber in central Italy. Hence, the combination of waterbborne TEM and SBP methods could offer a solution to improve the investigation of deep areas (resolved by TEM data), while lateral information can still be gained using SBP. The inclusion of SBP information for the interpretation of TEM data towards the inversion of an improved resistivity model, is an open area of research.

5.3.~~1~~2 ~~Sediment thickness estimation from~~Water-borne ~~TEM~~ transient electromagnetic ~~soundings~~method

The water-borne TEM sounding system ~~set up~~developed for this study turned out to provide reliable resistivity images for water depths down to at least 20 m. This conclusion is supported by the ~~good~~ agreement of the resistivity images obtained from water-borne TEM and lake-floor TDIP measurements along both TEM profiles (Fig. 7 and Fig. 10~~9~~). P~~It is worth mentioning that p~~revious shallow-water TEM studies (e.g., Butler, 2009; and references therein; Hatch et al., 2010; Mollidor et al., 2013) employed in-loop configurations with an outer transmitter loop and a smaller receiver loop or coil in the centre, while we used a light-weight single-loop configuration, which is quicker to assemble and easier to handle while navigating on the lake. It is worth mentioning that in terms of noise level and depth of investigation, our simple system consisting of one single circular loop provides comparable results as those obtained with more sophisticated systems consisting of separated transmitter and receiver square loops (e.g., Yogeshwar et al., 2020).

Besides the use of a single-loop configuration, the use of small loops as employed in the present study can eventually result in distortions in the transient data. The measured curves (truncated to 21.4–174.5 µs) do not show any conspicuous features (see data example in the appendix) and can be adjusted by reasonable resistivity models with an overall low root-mean-square (RMS) deviation. Thus, we discard the presence of such adverse effects in our data set. The good agreement between TEM and TDIP-derived resistivity models along collocated survey lines further supports this conclusion.

In the present study, TEM resistivity images clearly delineate the top of the bedrock and reveal the inner structure of the deltaic deposits of the river Nahá, which are not resolved by the SBP seismograms. The interpretation of the layered resistivity structure below the flat parts of the lake bottom is only possible by combining TEM resistivity images with complementary information from other methods. In particular, ~~However, our expectation that the electrically conductive fine grained sediments could be distinguished from the underlying resistive bedrock turned out to be inappropriate: While~~ the SBP

seismograms (and TDIP phase images) ~~lead to the conclusion~~imply that the thickness of the fine-grained lakebed sediments does not exceed 5-7 m in Lake Metzabok, while conductive units extend down to depths of 20-30 m (below the lake bottom) and more. -We resolve this apparent contradiction by postulating an intermediate layer made of limestone debris from collapsed karst cavities and fine-grained sediments filling the spaces between the limestone blocks. This mixed layer seems to be characterized by a much higher seismic velocity compared to the fine sediments but a similar or slightly lower electrical resistivity. Consequently, the small resistivity contrast between the fine-grained lakebed sediments and the underlying mixed layer hinders an unambiguous estimation of sediment thickness from TEM (and TDIP) resistivity data.

Our results also show the advantages in the interpretation of the sounding data after the incorporation of water depth and eventually water resistivity into the inversion of TEM data as a-priori information. Water depth is readily measured during the TEM sounding using a standard echo sounder. Further investigations can consider the addition of fluid conductivity and temperature measurements using conductivity-temperature-depth (CTD) probes to improve the inversion of waterborne measurements and, thus, the investigations of the lakebed by electrical methods. Such information can also be obtained from the analysis of water samples.

We have adjusted smooth and layered models to the TEM sounding data, both recovering similar sub-bottom structures along the two lines discussed here. While the smooth models facilitate a direct comparison with the (smooth) 2D TDIP resistivity images, the layered models are more appropriate to image sharp geological contacts. The average fit quality (as assessed by the percentage RMS), which is slightly better for the layered models, could point to rather sharp contacts. However, it is not at all straight forward to decide whether sharp resistivity contrasts exist between the main lithological units (i.e., sediment cover and limestone) or not. As our interpretation of the Metzabok data suggests, e.g., within the mixed layer, there might be a smooth transition due to a continuously increasing volume content of limestone with depth. The same is true for contacts between different, eventually interbedded sedimentary units (e.g., fine-grained lake sediments/sandy delta deposits).

~~**It is worth mentioning that previous shallow-water TEM studies (Butler, 2009; and references therein; Hatch et al., 2010; Mollidor et al., 2013) employed in-loop configurations with an outer transmitter loop and a smaller receiver loop or coil in the centre, while we used a single loop configuration, which is quicker to assemble and easier to handle while navigating on the lake. We also showed that it is sensible to constrain the interpretation of the sounding data by incorporating water depth and eventually water resistivity into the inversion process as a-priori information. Water depth is readily measured during the TEM sounding using a standard echo sounder. Further investigations can consider the addition of fluid conductivity and temperature measurements using conductivity-temperature-depth (CTD) probes to improve the inversion of waterborne measurements and, thus, the investigations of the lake bed by electrical methods. Such information can also be obtained from the analysis of water samples.**~~

5.3.2 Induced-polarization imaging of the lake floor

The fact that the studied lakes drained provided us with the unique opportunity to carry out TDIP measurements directly on the lake floor. The low contact resistances and the easy installation of electrodes on the soft ground represent ideal conditions for electrical imaging measurements. Furthermore, the evaluation of both phase data for sediment samples analysed in the

laboratory and for the in-situ measurements on the exposed lake floor is unprecedented or at least very rare in geophysical literature. In the present study, the TDIP phase results permitted to significantly improve the obtained geological model of the lake-bottom. In particular, the IP images showed a

~~Due to the~~ low phase response of the lake sediments on one hand and a~~the~~ comparably high phase response of the limestone bedrock ~~as well as~~and the collapse-debris layer on the other hand. ~~, the phase images obtained from TDIP data measured on the dry lake bottom turned out to be more conclusive for the delimitation of the layer of pure sediments than the resistivity images.~~ The interpretation of the field TDIP phases~~We conclu~~ is ~~de~~ sustained by ~~this from~~ the our laboratory measurements on sediment samples and the good overall agreement of the shallow low-phase layer with the corresponding reflector in the SBP images.

Larger variations in the phase response of sediments (especially the increased phase values of sample TZI19-A) are likely related to different depositional regimes: Preliminary geochemical analyses of the sediment samples imply significantly increased total organic carbon (TOC) and carbon-to-nitrogen ratio (C/N) of the sample TSI19-A compared to the other five samples (P. Hoelzmann, personal communication). High values of TOC and C/N point to a larger fraction of organic matter from terrestrial sources in sample TZI19-A, while the smaller amount of organic matter of the other five samples probably stems from algal plants. A strong control of TOC on the phase response has been reported earlier for other materials (e.g., Schwartz and Furman, 2015; Flores Orozco et al., 2020).

Based on the encouraging findings of the present study, the application of TDIP imaging for the lake-bottom characterization emerges as an interesting complementary method for the characterization of lake-bottom sediments. Although promising for desiccated or shallow lakes, there are some limitations for TDIP

~~Although this is definitely an interesting result, the practical relevance of this finding for~~ measurements to be carried out on water-filled lakes~~ would still have to be tested~~: In principle, TDIP data could be collected with floating electrode arrays as used for water-borne direct-current resistivity surveys. However, the collection of deep IP data - as needed to investigate the sediments below a water column of, e.g., 20 m – often suffers from a low S/N ratio. This limitation could ~~possibly~~ be overcome by bringing the electrodes closer to the lake bottom, which is possible but logistically more effortful (e.g., Baumgartner and Christensen, 2006).

5.3.4 Seismic refraction tomography of the lake floor

In the present study, the land SRT measurements carried out on the exposed lake floor confirmed the layered structure of the flat parts of the bottom of Lake Metzabok inferred from the preceding three methods. In those cases, where the depth of investigation of the SRT images was large enough to cover the top of the limestone bedrock (i.e., Profiles 2 and 4), this geological contact was delineated clearly by a steep increase in the SRT velocity model. The main limitations regarding the applicability of SRT measurement on the lake floor, which we identified in this study, are related to the specific surface conditions: On the one hand, the generation of seismic pulses was excessively labour intensive, as the steel plate bogged down into the soft lake-bottom and had to be dug out after every single hit. On the other hand, the low signal-to-noise (S/N) ratio of

some data collected on the muddy lake floor (e.g., along Profile 2, see appendix), rendered the processing and interpretation of SRT results challenging. We attribute the low S/N to the difficult coupling of seismic energy into the ground, a high energy loss of seismic signals in soft sediments, and a higher level of ambient noise (e.g., induced by wind). Although the picking percentages of noisy SRT profiles (here, Profile 2) were much lower and RMS deviations significantly increased in comparison to data collected on firm ground (e.g. Profile 5), the depth of investigation only decreased by approx. 20% (see Figs. 5c and 7d).

~~**5.3 Seismic versus electrical surveys**~~

~~For shallow water applications, the compact and mobile experimental setup as well as the high productivity and resolution in combination with the straight forward interpretation of the SBP lead to the conclusion that reflection seismic methods will probably not be substituted by TEM surveys. The latter are by far slower and more labour intensive in the field and in the office, and the resulting imaging results have a lower resolution. However, under the given geological conditions in the study area, waterborne TEM soundings have proven to work well and provide relevant complementary data. In our study, waterborne TEM soundings allowed to delineate the collapse-debris layer between fine-grained lakebed sediments and bedrock.~~

~~The situation is different when measurements have to be carried out directly on the bed of a dry lake: There, the muddy surface results in a high energy loss of seismic signals, which considerably decreases the quality of seismic data (as, e.g., reflected by a low picking percentage) and makes the application of SRT methods challenging. At the same time, the low contact resistances and the easy installation of electrodes on the soft ground represent ideal conditions for electrical imaging measurements. Therefore, it is not surprising that both productivity and data quality are higher for TDIP than for SRT measurements. The good agreement of our electrical data with co-located seismic reflection data (SBP), suggests that under certain conditions electrical surveys can eventually replace seismic surveys, especially if phase data is available.~~

6. Conclusions

Based on the combination of different geophysical techniques ~~field data collected on two karst lakes~~, the present study provides important insight into the geological situation of two hydraulically highly dynamic karst lakes~~investigates~~. The comparison of water-borne and land surveys (carried out after the sudden drainage of the lakes) permits a detailed evaluation of the potential and limitations of different seismic, electrical, and electromagnetic geophysical methods for the ~~reconnaissance of the bottom of~~ investigation of such~~shallow~~ lakes ~~and their sedimentary infill~~. One principal outcome of this study is that only the combination of complementary methods provides sufficient information to develop a comprehensive geological model of complex karst environments. In this sense, the present systematic field study paves the way towards an improved geophysical characterization, which is needed to better understand surface-groundwater interactions in karst systems and, more importantly, to evaluate climate-change related effects on karst water resources. In this regard, the interpretation of our results permitted to determine suitable drilling locations for future paleoenvironmental drilling campaigns, which are characterized by thick (5-6

m), undisturbed fine-grained lake sediments covering the flat parts of both studied lakes. The recovery of continuous and far-reaching sedimentary records is another important element for the understanding of the impact of climate change on the availability and quality of water in karst systems.

-The evaluation of the different methods derived substantial benefit from the possibility to recollect additional data directly on the exposed lake floor after the sudden drainage of Lakes Metzabok and Tzibaná. The good agreement of electrical resistivity data collected with a new water-borne TEM system, TDIP resistivity data ~~collected directly on~~from -the dry lake bottom, and electrical measurements on sediment samples in the laboratory demonstrates that the new ~~proposed~~ TEM system -works well down to water depths of at least 20 m. Furthermore, there is no reason to assume that the system should not work as well in even deeper water (>20 m) depending on the water conductivity.– TDIP phase images turned out to provide relevant complementary information – here, in particular about the inner structure of the conductive units covering the lake bottom. Seismic data from a water-borne SBP and a SRT survey on the dry lake floor provided complementary information and allowed to interpret the two conductive units as a top layer of fine-grained sediments and an intermediate layer of debris from collapsed cavities in the heavily karstified limestone bedrock. At the same time, the delineation of the upper limit of the buried limestone bedrock was not possible from the seismic data only. Thus, the final interpretation was only possible by combining electrical and seismic data sets and by incorporating geological and geomorphological constraints, showing – once again – the strength of a multi-methodological and interdisciplinary approach.

Appendix A: Data quality and filtering

TEM. Figure A.1a shows the TEM raw data of selected soundings along Profile 6 of Lake Tzibaná in terms of the induced voltage (normalized to loop area and transmitter current). As described in the main text, all sounding curves were truncated to a unit time window between 21.4 and 174.5 µs. Earlier times were ignored to minimize the effect of distorted early-time data. At the latest time window, the SEM of the induced voltage is approximately $5 \cdot 10^{-9}$ V/Am^2 for all soundings (except for TZI44) and about 1–2 orders magnitude smaller than the corresponding induced voltage. Figure A.1b shows the measured and calculated apparent resistivity curves of the same soundings. As indicated by the overall small root-mean-square error (RMS<5%), the measured curves are all recovered well by the adjusted smooth resistivity models, which are visualised in Fig. 10.

TDIP. TDIP data was filtered based on the apparent resistivity and apparent chargeability data. In a first step, TDIP readings with apparent resistivity values ≤0 Ωm and/or apparent chargeability values ≤0 mV/V were removed as outliers. In a second step, based on the visual assessment of the raw data pseudo sections and histograms (see Fig. A2 for an exemplary data set), measurements with apparent chargeability values >8 mV/V were removed as further outliers. The selection of the limit of 8 mV/V for the apparent chargeability values is based on the observation of a narrow distribution of physically meaningful values in the corresponding histograms (see Fig. A2 d and h). In the case of the data set shown in Fig A2, which corresponds to the second part of the roll-along profile 1 of Lake Metzabok, this filtering results in a reduction to 57% of the unfiltered data

set. This high loss of data is related to a comparably poor data quality of the chargeability measurements along this long line (470 m length, 10 m electrode spacing). Shorter profiles with half the electrode spacing (5 m in the case of profiles 2-4 and 6) are less affected by noisy chargeability data as reflected in a higher percentage of useful data (up to ~88% in the case of Profile 3 of Lake Metzabok).

SRT. Collected with 24 geophones and 25 shot positions, each tomographic data set consists of a total of 600 seismic traces. Fig. A3 shows exemplary seismic traces for one central shot positions and the travel-time curves (constructed from the picked first arrivals of all 25 shot positions) for one relatively noisy (Profile 2) and one relatively clean (Profile 4) data set. The picking percentage displayed along with the travel-time curves reflects the number of traces, for which a first arrival could be identified, and serves as a measure of overall data quality. The low data quality of Profile 2 data results in a low picking percentage (341 out of a total of 600 traces) and mainly affects long-offset data, which clearly reduces the depth of investigation (~40 m, Fig. 5c). In comparison, SRT data collected along Profile 4 is cleaner (552 first out of 600 first arrivals picked) and, thus, results in a larger depth of exploration (>50 m, Fig. 7d).

Data availability

All raw and processed data of this study (and some additional data not discussed here) are available at Zenodo (https://doi.org/10.5281/zenodo.3782402) along with the Matlab scripts used to prepare the visualizations presented in this manuscript.

Author contributions

AFO, JG, JH, WM, EG, and JR participated in the field seasons, which were planned and coordinated by MB, LP, AFO, CP, AH, and AS. RG and JH were responsible for the sediment and water samples and the laboratory IP data. CP, EG, and JR processed the SBP data. AFO processed and inverted the TDIP data, MS the SRT data, and LA the TEM data. WM made a geological field survey and gave insights into the geological context. JB prepared the maps and participated in the geological contextualization. All authors participated in the interpretation and discussion of the results. MB lead the redaction of the manuscript with contributions of all co-authors.

Competing interests

The authors declare that they have no conflict of interest.

Acknowledgements

We thank the Comisión Nacional de Áreas Naturales Protegidas (CONANP) and the authorities of the protected area Nahá and Metzabok, in particular Sergio Montes Quintero, Santiago Landois Álvarez Icaza, Miguel García Cruz, Rafael Tarano, and José Ángel Solórzano, as well as the municipalities of Nahá and Metzabok for their openness and friendly support. We are grateful for the help provided by Mauricio Bonilla, Johannes Bücker, Martín Garibay, Carlos Cruz, Roberto Reyes, Lorena Bárcena, Rodrigo Martínez Abarca, and Theresia Lauke, and all other colleagues and students, who were actively involved during the field seasons. Finally, we would like to thank Socorro Lozano, Margarita Caballero, Beatriz Ortega, Sergio Rodríguez, and Alex Correa Metrio from the Institutes of Geology and Geophysics, UNAM, for institutional and logistical support. We also thank Pritam Yogeshwar and one anonymous reviewer for their thoughtful revisions, which helped to significantly improve the present manuscript.

Financial support

Financial support was provided by Consejo Nacional de Ciencia y Tecnología (CONACyT) under grant number 252148 and Deutsche Forschungsgemeinschaft (DFG) under grant numbers BU3911/1-1 and PE2133/1-1. Parts of this work were funded through the Austrian Science Fund (FWF) – Agence Nationale de la Recherche (ANR) research project FWF-I-2619-N29 and ANR-15-CE04-0009-01 HYDROSLIDE: Hydro-geophysical observations for an advanced understanding of clayey landslides as well as by the Austrian Federal Ministry of Science, Research and Economy (project: ExploGRAF- Development of geophysical exploration methods for the characterization of mine-tailings towards exploitation).

References

Bairlein, K., Hördt, A., and Nordsiek, S.: The influence on sample preparation on spectral induced polarization of unconsolidated sediments, Near. Surf. Geophys., 12(5), 667-678, https://doi.org/10.3997/1873-0604.2014023, 2014.

Barrière, J., Bordes, C., Brito, D., Sénéchal, P., and Perroud, H.: Laboratory monitoring of P waves in partially saturated sand, Geophys. J. Int., 191(3), https://doi.org/10.1111/j.1365-246X.2012.05691.x, 1152-1170, 2012.

Baumgartner, F., and Christensen, N.B.: Analysis and application of a non-conventional underwater geoelectrical method in Lake Geneva, Switzerland. Geophys. Prospect., 46(5), 527-541. https://doi.org/10.1046/j.1365-2478.1998.00107.x, 2006.

Befus, K. M., Cardenas, M. B., Ong, J. B., and Zlotnik, V. A.: Classification and delineation of groundwater–lake interactions in the Nebraska Sand Hills (USA) using electrical resistivity patterns. Hydrogeology Journal, 20(8), 1483-1495, https://doi.org/10.1007/s10040-012-0891-x, 2012.

Binley, A., and Kemna, A.: DC resistivity and induced polarization methods, in: Hydrogeophysics, edited by Rubin, Y., and Hubbard, S.S., Springer Netherlands, Dordrecht, Netherlands,129–156, https://doi.org/10.1007/1-4020-3102-5_5, 2005.

Bücker, M., Lozano-Garcia. S., Ortega-Guerrero, B., Caballero-Miranda, M., Pérez, L., Caballero, L., Pita de la Paz, C., Sánchez-Galindo, A., Jesús Villegas, F., Flores Orozco, A., Brown, E., Werne, J., Valero Garcés, B., Schwalb, A., Kemna, A., Sánchez-Alvaro, E., Launizar-Martínez, N., Valverde-Placencia, A., and Garay-Jiménez, F.: Geoelectrical and Electromagnetic Methods Applied to Paleolimnological Studies: Two Examples from Desiccated Lakes in the Basin of Mexico, B. Soc. Geol. Mex., 69(2), 279-298, http://dx.doi.org/10.18268/bsgm2017v69n2a1, 2017.

Butler, K. E.: Trends in waterborne electrical and EM induction methods for high resolution sub-bottom imaging, Near. Surf. Geophys., 7(4), 241-246, https://doi.org/10.3997/1873-0604.2009002, 2009.

Charqueño Celis, N.F., Garibay, M., Sigala, I., Brenner, M., Echeverria-Galindo, P., Lozano, S., Massaferro, J., and Pérez L.: Testate amoebae (Amoebozoa: Arcellinidae) as indicators of dissolved oxygen concentration and water depth in lakes of the Lacandón Forest, southern Mexico: Testate amoebae from Lacandón Forest lakes, Mexico, J. Limnol., 79(1), 82-91, https://doi.org/10.4081/jlimnol.2019.1936, 2020.

Cohen, A. S.: Paleolimnology: the history and evolution of lake systems, Oxford University Press, New York, USA, 528 pp., 2003.

~~Cohuo, S., Macario-González, L., Pérez, L., Sylvestre, F., Paillès, C., Curtis, J. H., Kutterolf, S., Wojewódka, M., Zawisza, E., and Schwalb, A.: Climate ultrastructure and aquatic community response to Heinrich Stadials (HS5a-HS1) in the continental northern Neotropics, Quaternary Sci. Rev. 197, 75-91., https://doi.org/10.1016/j.quascirev.2018.07.015, 2018.~~

Colombero, C., Comina, C., Gianotti, F., and Sambuelli, L.: Waterborne and on-land electrical surveys to suggest the geological evolution of a glacial lake in NW Italy, J. Appl. Geophys., 105, 191-202, https://doi.org/10.1016/j.jappgeo.2014.03.020, 2014.

Dahlin, T., Leroux, V., and Nissen, J.: Measuring techniques in induced polarisation imaging, J. Appl. Geophys., 50(3), 279-298, https://doi.org/10.1016/S0926-9851(02)00148-9, 2002.

Díaz, K. A., Pérez, L., Correa-Metrio, A., Franco-Gaviria, J. F., Echeverría, P., Curtis, J., and Brenner, M.: Holocene environmental history of tropical, mid-altitude Lake Ocotalito, México, inferred from ostracodes and non-biological indicators, The Holocene 27, 1308-1317, https://doi.org/10.1177/0959683616687384, 2017.

Dondurur, D.: Acquisition and processing of marine seismic data, Elsevier, Netherlands, United Kingdom, United States, 606 pp., https://doi.org/10.1016/C2016-0-01591-7, 2018.

Echeverría Galindo, P.G., Pérez, L., Correa-Metrio, A., Avendaño, C., Moguel, B., Brenner, M., Cohuo, S., Macario, L., Schwalb, A.: Tropical freshwater ostracodes as environmental indicators across an altitude gradient in Guatemala and Mexico. Rev. Biol. Trop., 67, 1037-1058, https://doi.org/10.15517/rbt.v67i4.33278, 2019.

Flores Orozco, A., Bücker, M., Steiner, M., and Malet, J.P.: Complex-conductivity imaging for the understanding of landslide architecture, Eng. Geol., 243, 241-252, https://doi.org/10.1016/j.enggeo.2018.07.009, 2018a.

Flores Orozco, A., Gallistl, J., Bücker, M., and Williams, K. H.: Decay curve analysis for data error quantification in time-domain induced polarization imaging, Geophysics, 83(2), E75-E86, https://doi.org/10.1190/geo2016-0714.1, 2018b.

Flores-Orozco, A., Gallistl, J., Steiner, M., Brandstätter, C., and Fellner, J.: Mapping biogeochemically active zones in landfills with induced polarization imaging: The Heferlbach landfill, Waste Manage., 107, 121-132, https://doi.org/10.1016/j.wasman.2020.04.001, 2020.

Ford, D. C., and Williams, P. W.: Karst Hydrogeology and Geomorphology, Wiley, Chichester, 2007.

García-Gil, J.G., and Lugo Hupb, J.: Las formas del relieve y los tipos de vegetación en la Selva Lacandona. in: Reserva de la Biósfera Montes Azules, Selva Lacandona: Investigación para su conservación, edited by: Vásquez-Sánchez, M.A., and Ramos Olmos, M. A., Centro de Estudios para la Conservación de los Recursos Naturales, San Cristóbal de las Casas, Mexico, 39-49, 1992.

Hartmann, A., Goldscheider, N., Wagener, T., Lange, J., and Weiler, M.: Karst water resources in a changing world: Review of hydrological modeling approaches, Rev. Geophys., 52(3), 218-242, https://doi.org/10.1002/2013RG000443, 2014.

Hatch, M., Munday, T., and Heinson, G.: A comparative study of in-river geophysical techniques to define variations in riverbed salt load and aid managing river salinization, Geophysics, 75(4), WA135-WA147, https://doi.org/10.1190/1.3475706, 2010.

Kaufman, A. A., Alekseev, D., Oristaglio, M.: Principles of electromagnetic methods in surface geophysics, 45, Elsevier, Amsterdam, Netherlands, 770 p, 2014.

Kemna, A.: Tomographic inversion of complex resistivity - theory and application, Ph.D., Ruhr-University of Bochum, Bochum, Germany, 176 pp., 2000.

Kemna, A., E. Räkers, and Dresen, L..: Field applications of complex resistivity tomography, in: 69th Annual International Meeting, SEG, Expanded Abstracts, Houston, United States, 31 November – October 31 1999, 331–334, https://doi.org/10.1190/1.1821014, 1999.

Kozola, S.: Large Data in MATLAB: A Seismic Data Processing Case Study, MATLAB Central File Exchange, https://www.mathworks.com/matlabcentral/fileexchange/30585-large-data-in-matlab-a-seismic-data-processing-case-study, 2011.

Kruschwitz, S.: Assessment of the complex resistivity behavior of salt affected building materials, Ph.D., Technical University of Berlin, Berlin, Germany, https://doi.org/10.14279/depositonce-1722, 2007.

Lane Jr, J. W., Briggs, M. A., Maurya, P. K., White, E. A., Pedersen, J. B., Auken, E., Terry, N., Minsley, B., Kress, W. LeBlanc, D. R., Adams, R., and Johnson, C. D.: Characterizing the diverse hydrogeology underlying rivers and estuaries using new floating transient electromagnetic methodology, Sci. Total Environ., 140074, https://doi.org/10.1016/j.scitotenv.2020.140074, 2020.

Last, W.M., and Smol, J. P.: An introduction to basin analysis, coring and chronological techniques used in paleolimnology, in: Tracking Environmental Change Using Lake Sediments. Developments in Paleoenvironmental Research, edited by: W.M., Smol J. P., Springer, Dordrecht, Netherlands, 1–5, https://doi.org/10.1007/0-306-47669-X_1, 2002.

Lozada Toledo, J.: Usos del agua entre los lacandones de Metzabok, Ocosingo, Chiapas. Un análisis de Ecología Histórica, M.S., El Colegio de la Frontera Sur, San Cristobal de las Casas, Chiapas, Mexico, 261 pp., 2013.

Lozano-García, S., Brown, E. T., Ortega, B., Caballero, M., Werne, J., Fawcett, P. J., Schwalb, A., Valero-Garcés, B., Schnurrenberger, D., O´Grady, R., Stockhecke, M., Steinman, B., Cabral-Cano, E., Caballero, C., Sosa-Nájera, S., Soler, A. M., Pérez, L., Noren, A., Myrbo, A., Bücker, M., Wattrus, N., Arciniega, A., Wonik, T., Watt, S., Kumar, D., Acosta, C., Martínez, I., Cossio, R., Ferland, T., Vergara-Huerta, F.: Perforación profunda en el lago de Chalco: reporte técnico, B. Soc. Geol. Mex. 69, 299-311, http://dx.doi.org/10.18268/bsgm2017v69n2a2, 2017.

Mandujano-Velazquez, J. J., and Keppie, J. D.: Middle Miocene Chiapas fold and thrust belt of Mexico: a result of collision of the Tehuantepec Transform/Ridge with the Middle America Trench. Geol. Soc. Spec. Publ. 327(1), 55-69, https://doi.org/10.1144/SP327.4, 2009.

Medina-Elizalde, M., and Rohling, E. J.: Collapse of Classic Maya civilization related to modest reduction in precipitation, Science, 335(6071), 956-959, https://doi.org/10.1126/science.1216629, 2012.

Mollidor, L., Tezkan, B., Bergers, R., and Löhken, J.: Float-transient electromagnetic method: in-loop transient electromagnetic measurements on Lake Holzmaar, Germany. Geophysical Prospecting, 61(5), 1056-1064, https://doi.org/10.1111/1365-2478.12025, 2013.

Orlando, L.: Some considerations on electrical resistivity imaging for characterization of waterbed sediments, J. Appl. Geophys., 95, 77-89, https://doi.org/10.1016/j.jappgeo.2013.05.005, 2013.

Pelton, W. H., Ward, S. H., Hallof, P. G., Sill, W. R., and Nelson, P. H.: Mineral discrimination and removal of inductive coupling with multifrequency IP, Geophysics, 43(3), 588-609, https://doi.org/10.1190/1.1440839, 1978.

Pérez, L., Correa-Metrio, A., Cohuo, S., Macario-González, L., Echeverría-Galindo, P., Brenner, M., Curtis, J., Kutterolf, S., Stockhecke, M., Schenk, F., Bauersachs, T., and Schwalb A.: Ecological turnover in Neotropical freshwater and terrestrial communities during episodes of abrupt climate change, Quaternary Res., accepted November 2020 (reference to be completed for final submission).

~~Pérez, L., Bugja, R., Lorenschat, J., Brenner, M., Curtis, J., Hoelzmann, P., Islebe, G., Scharf, B., and Schwalb, A.: Aquatic ecosystems of the Yucatán Peninsula (Mexico), Belize, and Guatemala, Hydrobiologia 661, 407-433, https://doi.org/10.1007/s10750-010-0552-9, 2011.~~

Reynolds, J. M.: An introduction to applied and environmental geophysics, John Wiley and Sons, Oxford, United Kingdom, 710 pp., 2011.

Ronczka, M., Hellman, K., Günther, T., Wisén, R., and Dahlin, T.: Electric resistivity and seismic refraction tomography: a challenging joint underwater survey at Äspö Hard Rock Laboratory, Solid Earth, 8(3), 671, https://doi.org/10.5194/se-8-671-2017, 2017

Rubio Sandoval, C. Z.: Estudio paleoambiental en dos lagos kársticos de la Selva Lacandona, Chiapas, Mexico, durante los últimos ~500 años utilizando indicadores biológicos y geoquímicos, M.S., Universidad Nacional Autónoma de México, Mexico City, Mexico, 117 pp., 2019.

Rücker, C., Günther, T., Wagner, F. M.: pyGIMLi: An open-source library for modelling and inversion in geophysics, Computers and Geosciences, 109, 106-123, https://doi.org/10.1016/j.cageo.2017.07.011, 2017.

Schindler, D.W.: Lakes as sentinels and integrators for the effects of climate change on watersheds, airsheds, and landscapes, Limnol. Oceanogr., 54(6), 2349, https://doi.org/10.4319/lo.2009.54.6_part_2.2349, 2009.

Scholz, C. A.: Applications of seismic sequence stratigraphy in lacustrine basins, in: Tracking Environmental Change Using Lake Sediments. Developments in Paleoenvironmental Research, edited by: W.M., Smol J. P., Springer, Dordrecht, Netherlands, 7–22, https://doi.org/10.1007/0-306-47669-X_2, 2002.

Schwartz, N. and Furman, A.: On the spectral induced polarization signature of soil organic matter, Geophys. J. Int., 200(1), 589–595, https://doi.org/10.1093/gji/ggu410, 2015.

~~Sigala, I., Caballero, M., Correa-Metrio, A., Lozano-García, S., Vázquez, G., Pérez, L., and Zawisza, E.: Basic limnology of 30 continental waterbodies of the Transmexican Volcanic Belt across climatic and environmental gradients, B. Soc. Geol. Mex. 69, 313–370, http://dx.doi.org/10.18268/bsgm2017v69n2a3, 2017.~~Spies, B. R.: Depth of investigation in electromagnetic sounding methods, Geophysics, 54, 872–888, https://doi.org/10.1190/1.1442716, 1989.

Toran, L., Nyquist, J., Rosenberry, D., Gagliano, M., Mitchell, N., and Mikochik, J.: Geophysical and hydrologic studies of lake seepage variability, Groundwater, 53(6), 841-850, https://doi.org/10.1111/gwat.12309, 2015.

Uyanık, O.: The porosity of saturated shallow sediments from seismic compressional and shear wave velocities, J. Appl. Geophys., 73(1), 1, https://doi.org/10.1016/j.jappgeo.2010.11.001, 2011.

Van Voorhis, G. D., Nelson, P. H., and Drake, T.L.: Complex resistivity spectra of porphyry copper mineralization, Geophysics, 38(1), 49-60, https://doi.org/10.1190/1.1440333, 1973.

Vázquez-Molina, Y., Correa-Metrio, A., Zawisza, E., Franco-Gaviria, J.F., Pérez, L., Romero, F., Prado, B., Charqueño-Celis, F., and Esperón-Rodríguez, M.: Decoupled lake history and regional climates in the middle elevations of tropical Mexico, Rev. Mex. Cienc. Geol., 33, 355-364, https://doi.org/10.22201/cgeo.20072902e.2016.3.450, 2016.

Waxman, M. H., and Smits, L. J. M.: Electrical conductivities in oil-bearing shaly sands, Soc. of Petrol. Eng. J., 8(02), 107-122, https://doi.org/10.2118/1863-A, 1968.

Weigand, M., Orozco, A. F., and Kemna, A.: Reconstruction quality of SIP parameters in multi-frequency complex resistivity imaging, Near. Surf. Geophys., 15(2), 187–199, https://doi.org/10.3997/1873-0604.2016050, 2017.

White, D. J.: Two-dimensional seismic refraction tomography, Geophys. J. Int., 97(2), 223-245, https://doi.org/10.1111/j.1365-246X.1989.tb00498.x, 1989.

Yogeshwar, P., Küpper, M., Tezkan, B., Rath, V., Kiyan, D., Byrdina, S., Cruz, J., Andrade, C., and Viveiros, F.: Innovative boat-towed transient electromagnetics Investigation of the Furnas volcanic lake hydrothermal system, Azores. Geophysics, 85(2), E41-E56, https://doi.org/10.1190/geo2019-0292.1, 2020.

Table 1: Ranges of physical properties of the geological units interpreted from our geophysical profiles and laboratory measurements. Resistivity data based on TEM, TDIP resistivity and laboratory measurements; phase data (absolute value) according to TDIP images and laboratory data between 1 und 10 Hz; p-wave velocity from SRT images.

Material / geological unit	Resistivity (Ωm)	Phase (mrad)	P-wave velocity (m/s)
Fine-grained sediments	~~10~~5 – ~~-~~30	<4	200 – ~~-~~1500
Collapse debris & fine-grained sediments	5 – ~~10~~ 20	>5 – ~~-~~6	1500 – ~~-~~2000
Limestone bedrock	>100	>4 – ~~-~~5	>2000

Table 2: Methods used to image the sub-bottom structure of the studied lakes. Summary of physical properties resolved, typical parameter ranges in the study area as well as setup and characteristics of the measurements. Typical depths of investigations depend on the specific instrumental setup used; main contributions and limitations mostly refer to the present study and the specific geological situation.

Method	Physical property and typical range	Setup and characteristics	DOI (m)	Main contribution	Main limitations
SBP	v_p* only reflection patterns resolved	Water borne; 10-kHz transducer, 300 W output power, boat	10	Resolves contact between fine-grained sediments and underlying mixed layer (e.g., Fig. 4e)	– Penetration depth ≤ 10 m below lake bottom (e.g., Fig. 4e) – No penetration in coarse delta sediments (e.g., Fig. 10a)
TEM	ρ** 5–500 Ωm	Water borne; unanchored single-loop system, 412 m² loop area, 1 A transmitter current, rubber boat	50–100	Delineates top of bedrock (e.g., Fig. 7a) and coarse delta deposits (e.g., Fig. 10a)	– Low acquisition velocity/productivity compared to SBP
TDIP	ρ 5–500 Ωm φ*** 2–6 mrad	Terrestrial; 5–10 m spacing, 48 electrodes, dipole-dipole, 0.5–1 A transmitter current, 500 ms pulse	50–70	ρ: Delineates coarse delta deposits (e.g., Fig. 10b) φ: Improved delineation of fine-grained sediments (e.g., Fig. 5b)	– No clear distinction between lake sediments and limestone bedrock if only ρ is considered (e.g., Fig. 4f)
SRT	v_p 200 – 3000 m/s	Terrestrial; 5 m spacing, 24 geophones (28 Hz), energy source: 7.5 kg sledge hammer	40–50	Delineates top of bedrock (e.g., Fig. 7d)	– Eventually low quality of data acquired on muddy lake floor

*p-wave velocity, **electrical resistivity, ***resistivity phase

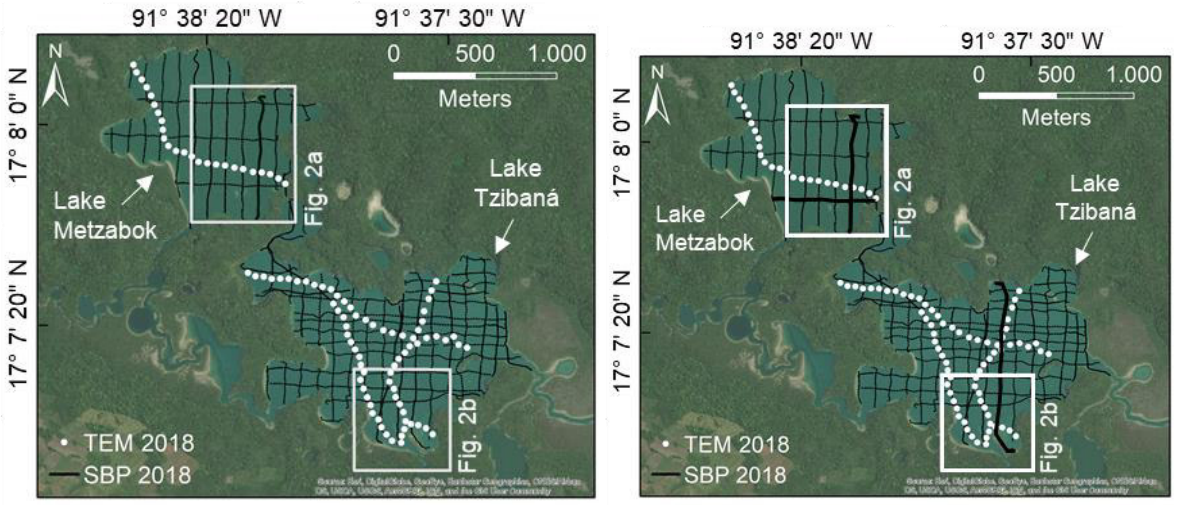

Figure 1: Layout of the geophysical survey on lakes Metzabok and Tzibaná during high-level stands in March 2018. Black lines show the sub-bottom profiler (SBP) survey grid, bold lines highlight those profiles discussed in detail in this manuscript, white circles represent individual transient electromagnetic soundings (TEM). The optical satellite image in the background (source: Bing Maps data base) shows lake water surface similar to the high-level stands encountered during March 2018.

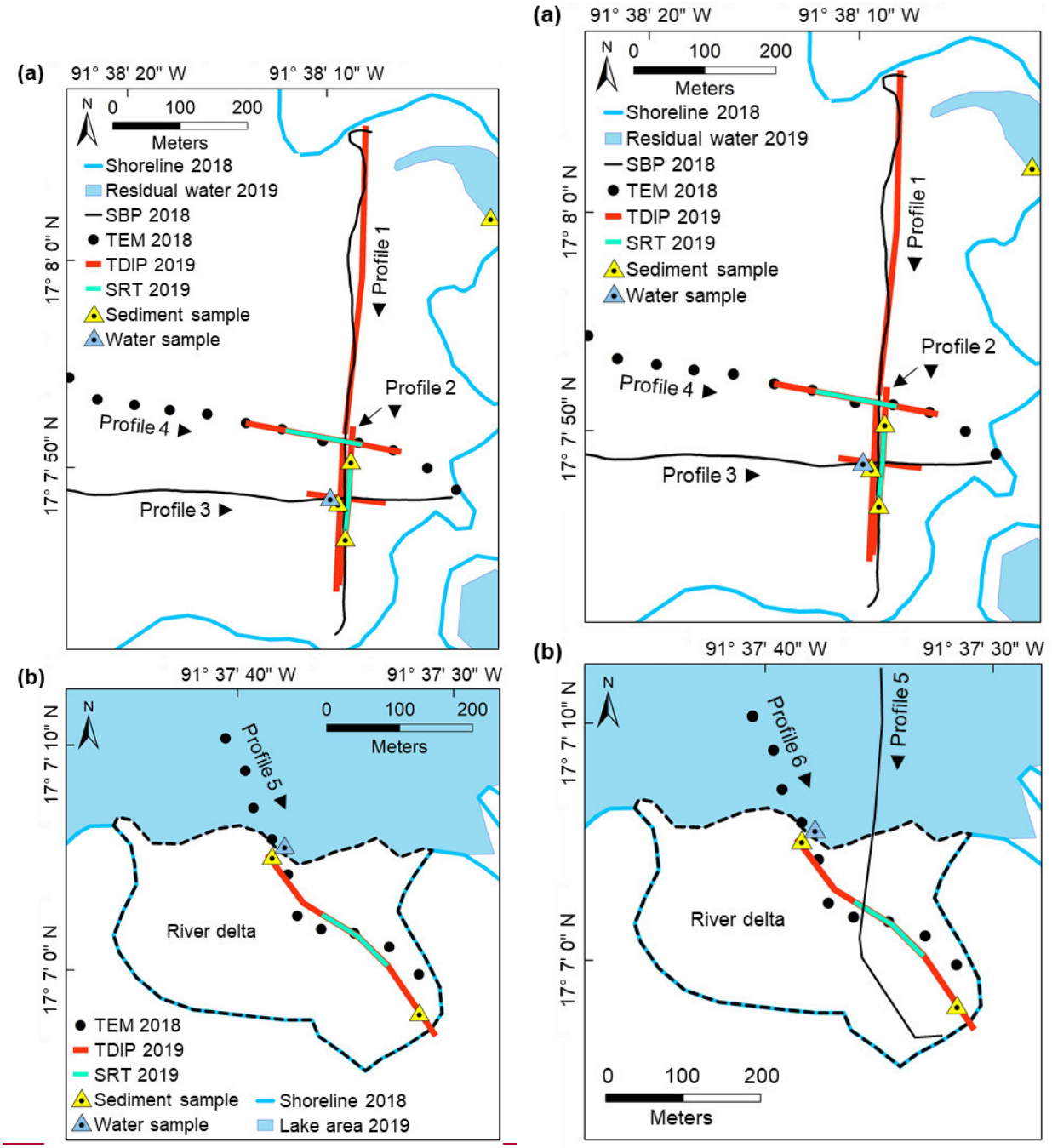

Figure 2: Layout of the geophysical survey on lakes Metzabok (a) and Tzibaná (b) in October 2019 (after the sudden lake-level drop) including sub-bottom profiler (SBP), transient electromagnetic (TEM), time-domain induced polarization (TDIP), and seismic refraction tomography (SRT) measurements. The geophysical measurements discussed here are grouped into five profiles; black triangles next to the profile names indicate the profile orientations. Yellow and blue triangles indicate sampling locations for sediment and water samples analysed in the laboratory, respectively. The dashed black line in (b) indicates the dry part of the river delta exposed during October 2019.

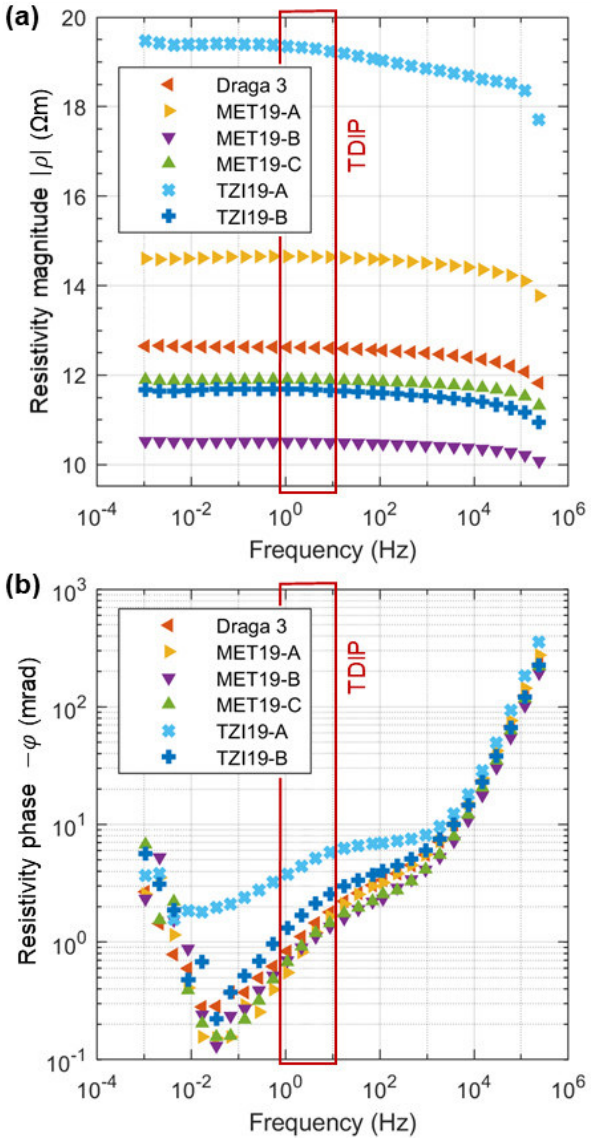

855 **Figure 3: Frequency-dependent complex resistivity of six lake-bottom sediment samples retrieved from Lake Metzabok (triangles) and Lake Tzibaná (crosses). Complex-resistivity values are given in terms of (a) magnitude and (b) phase. The highlighted frequencies between 1 and 10 Hz roughly correspond to the range tested by our time-domain induced polarization measurements in the field.**

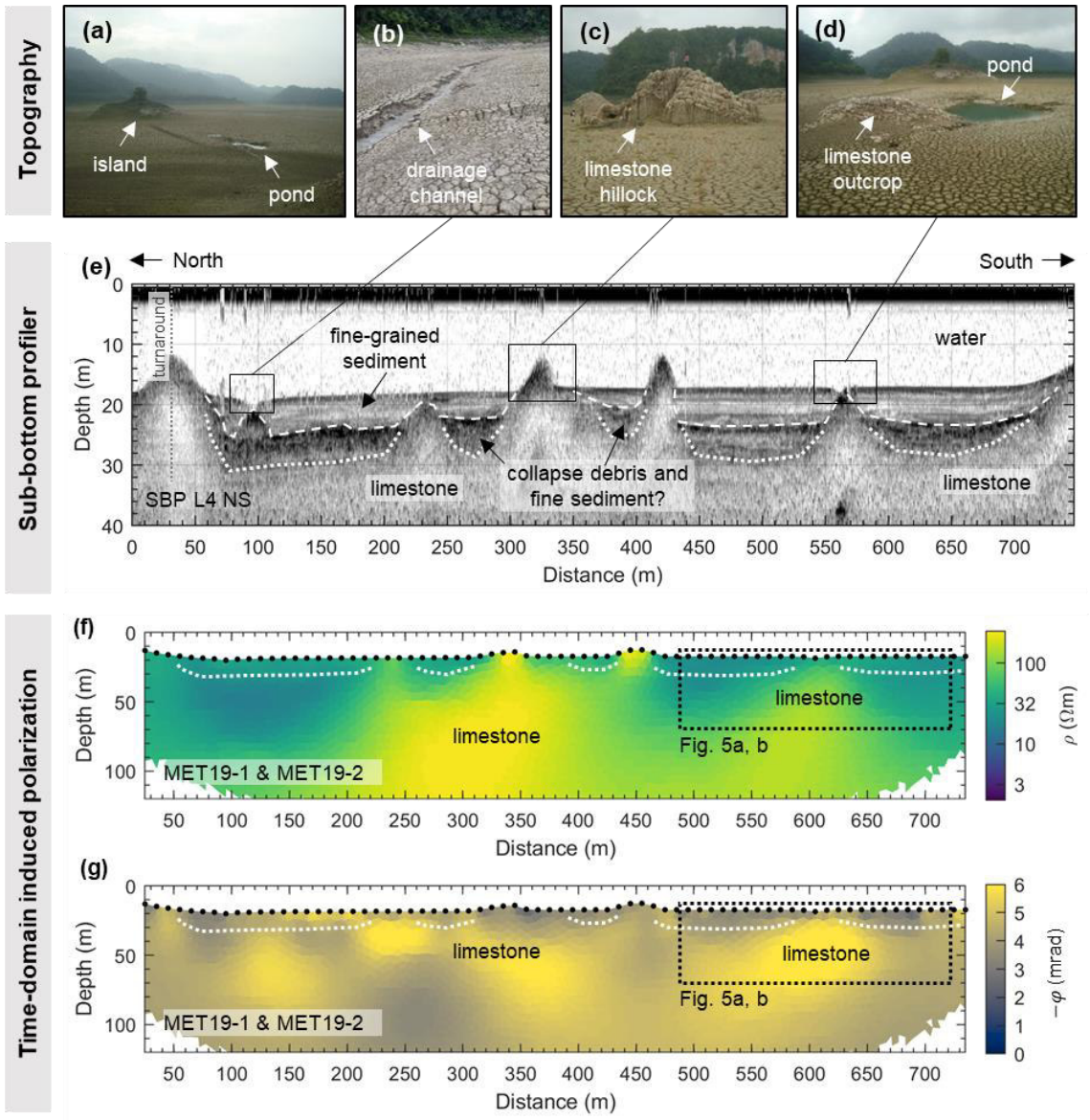
Topography
(a)
island
pond
(b)
drainage channel
(c)
limestone hillock
(d)
pond
limestone outcrop
Sub-bottom profiler
(e)
North
South
turnaround
fine-grained sediment
water
Depth (m)
SBP L4 NS
limestone
collapse debris and fine sediment?
limestone
Distance (m)
Time-domain induced polarization
(f)
limestone
limestone
Fig. 5a, b
MET19-1 & MET19-2
ρ (Ωm)
Distance (m)
(g)
limestone
limestone
Fig. 5a, b
MET19-1 & MET19-2
−φ (mrad)
Distance (m)

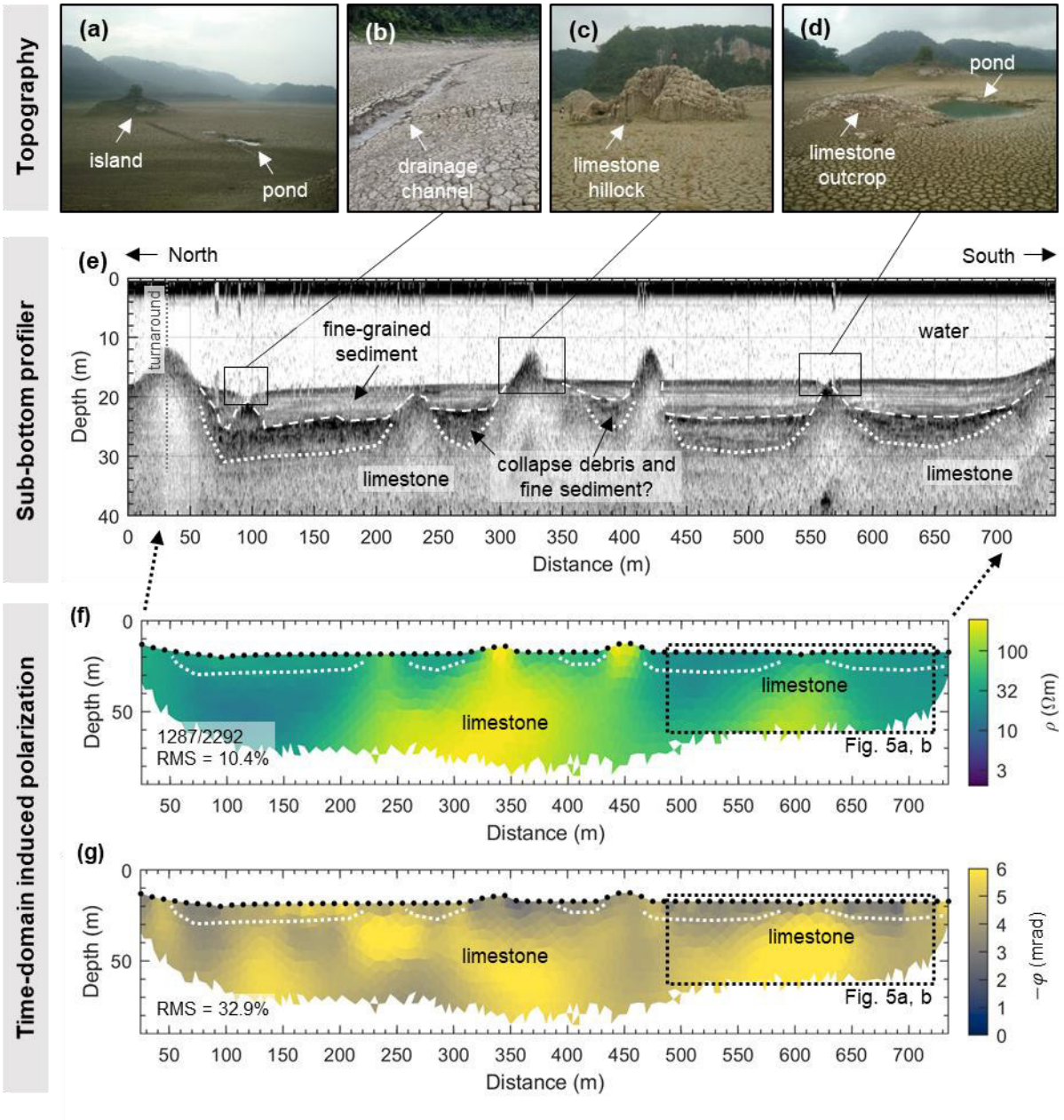

Figure 4: Topographic features and geophysical sections along Profile 1 of Lake Metzabok. Photographs of topographical features taken in October 2019: (a) lake basin with flat bottom, (b) drainage channel, (c) limestone hillock, (d) deep fracture and pond next to shallow limestone outcrop. (e) ~~s~~Sub-bottom profiler (SBP) section with dashed lines highlighting the main reflector encountered below the lake floor and dotted lines outlining a zone of high diffuse reflectivity, (f) and (g) electrical resistivity and phase images, respectively, including electrode positions (black dots along the surface) and dotted lines taken from SBP section. Electrical sections are shifted by 25 m with respect to the SPB section. Labels in the lower left corners of (f) and (g) represent the amount of data points used for the inversion compared to the total measured data (same for resistivity and phase) and the respective percentage root mean square deviations (RMS) of the inversion~~sections refer to the IDs within the data set published along this manuscript~~.

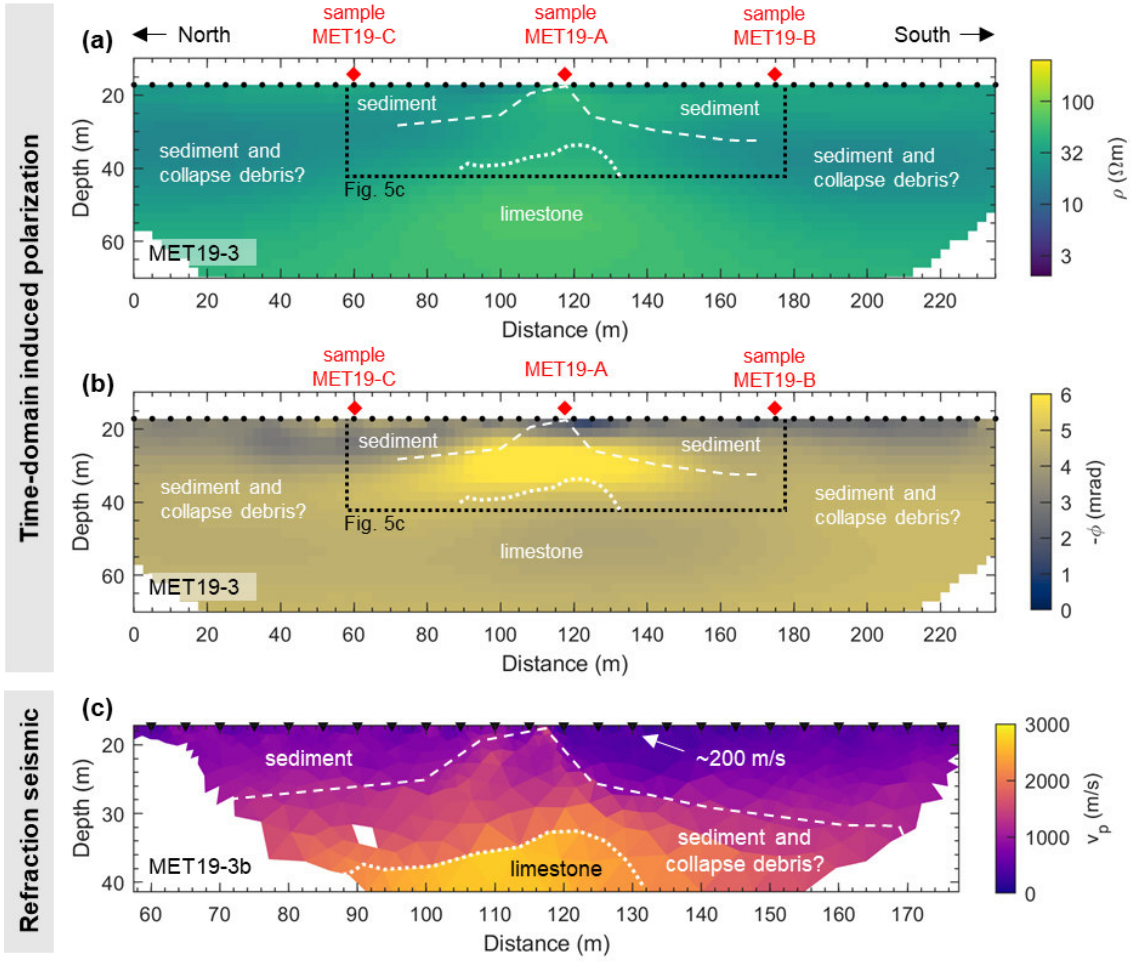
Time-domain induced polarization
Refraction seismic
(a)
North
South
sample MET19-C
sample MET19-A
sample MET19-B
sediment
sediment
sediment and collapse debris?
sediment and collapse debris?
Fig. 5c
limestone
MET19-3
Depth (m)
Distance (m)
ρ (Ωm)
100
32
10
3
(b)
sample MET19-C
MET19-A
sample MET19-B
sediment
sediment
sediment and collapse debris?
sediment and collapse debris?
Fig. 5c
limestone
MET19-3
Depth (m)
Distance (m)
-ϕ (mrad)
(c)
sediment
~200 m/s
sediment and collapse debris?
limestone
MET19-3b
Depth (m)
Distance (m)
v_p (m/s)
3000
2000
1000
0

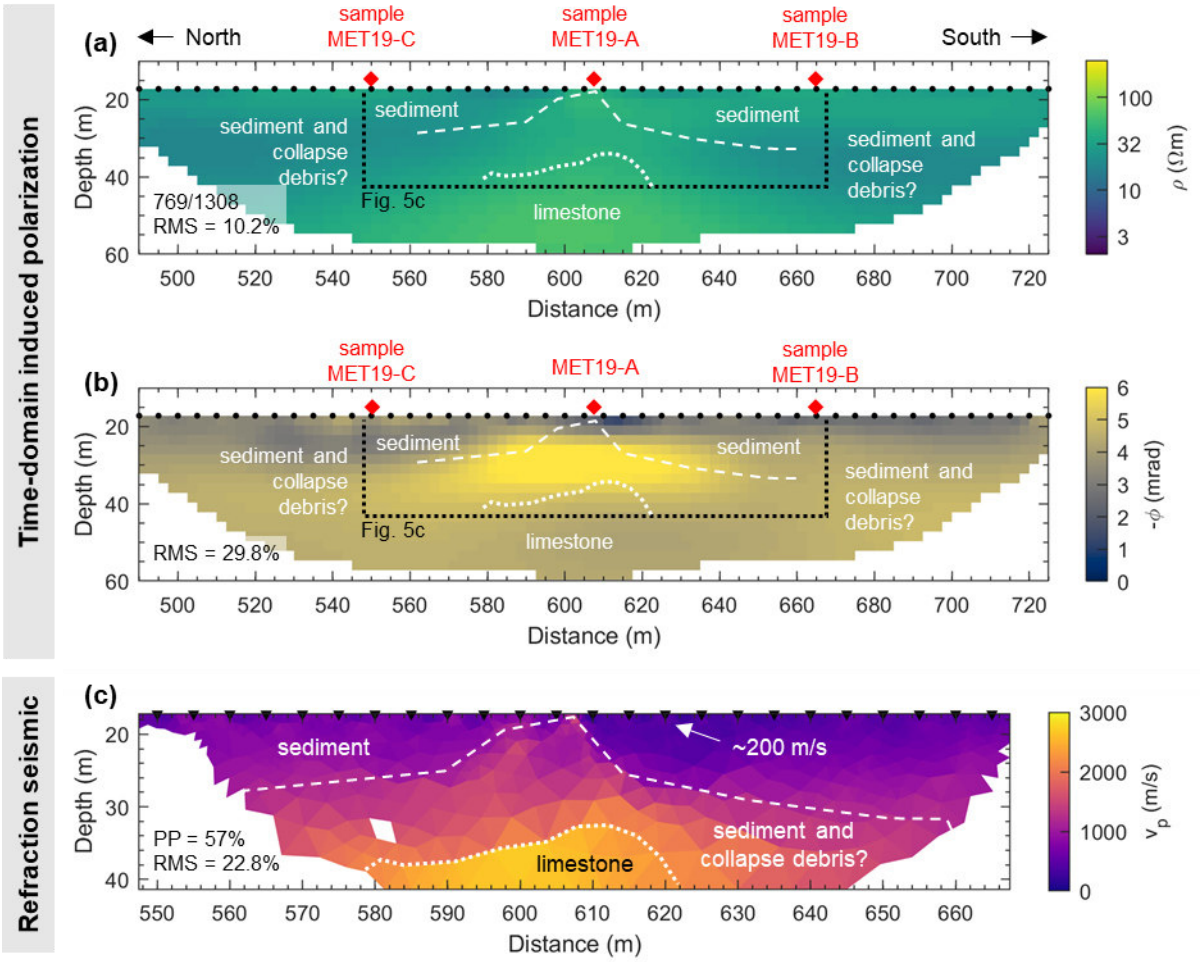

Figure 5: Geophysical sections along Profile 2 of Lake Metzabok (same coordinates as in Fig. 4): (a) and (b) electrical resistivity and phase images, respectively, including electrode positions (black dots along the surface), sampling locations of sediment samples (red diamonds at the surface), and the main lithological units interpreted from the SBP image (dotted lines). Labels in the lower left corners represent the amount of data points used for the inversion compared to the total measured data (same for resistivity and phase) and the respective percentage root mean square deviations (RMS) of the inversion. ~~;~~ (c) ~~s~~Seismic refraction tomogram with main lithological units including picking percentage (PP) and RMS of the inversion.

~~**Labels in the lower left corners of the sections refer to the IDs within the data set published along this manuscript.**~~

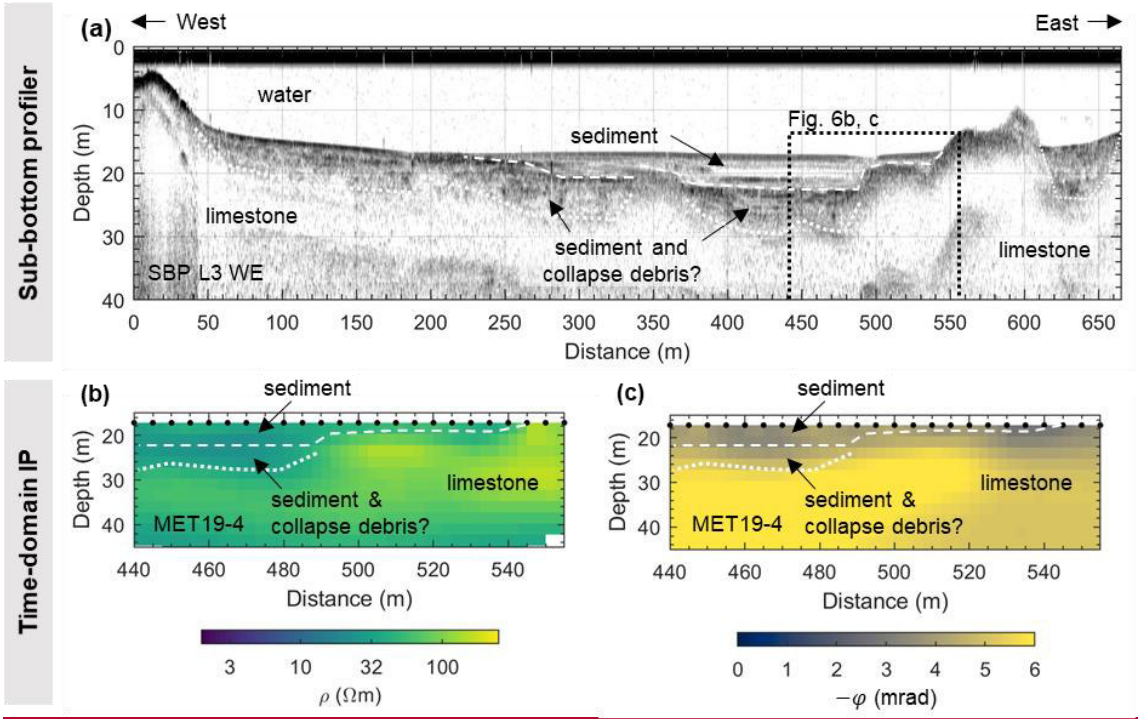
Sub-bottom profiler
(a)
West
East
water
sediment
Fig. 6b, c
limestone
sediment and
collapse debris?
limestone
SBP L3 WE
Depth (m)
Distance (m)
Time-domain IP
(b)
(c)
sediment
limestone
sediment &
collapse debris?
MET19-4
Distance (m)
3 10 32 100
ρ (Ωm)
0 1 2 3 4 5 6
−φ (mrad)

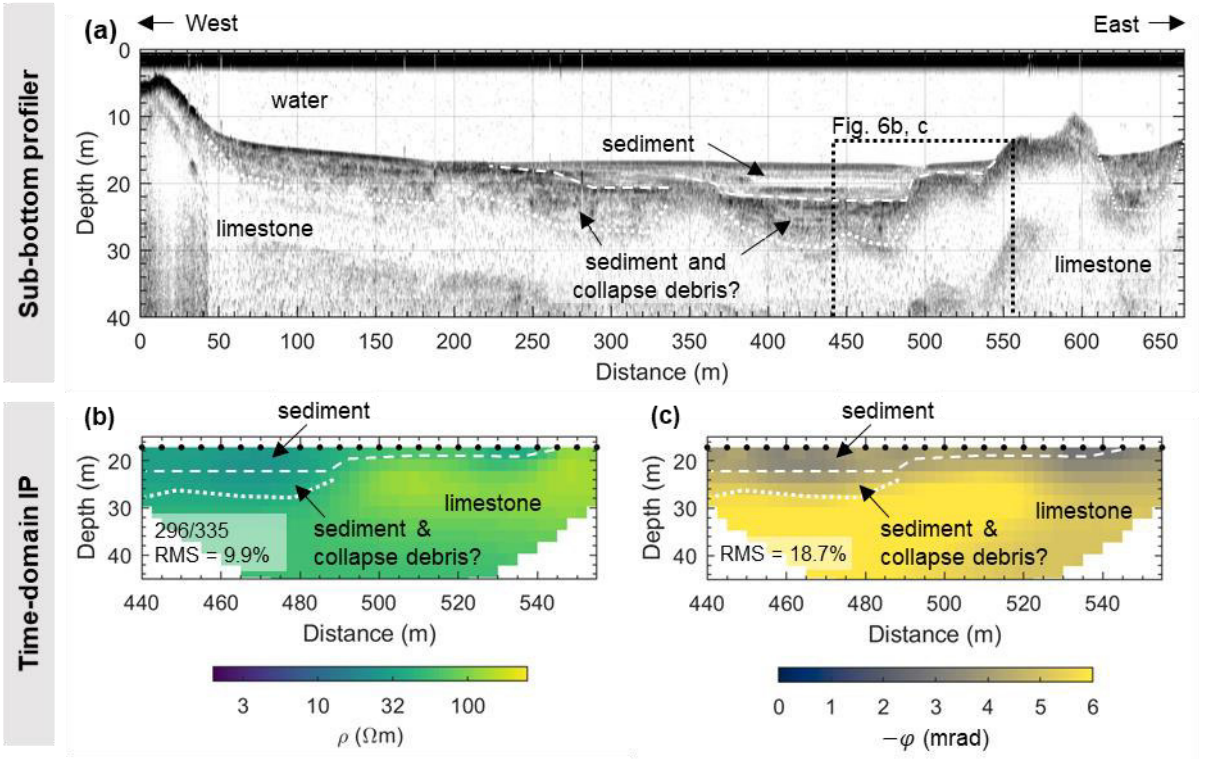
Sub-bottom profiler
(a)
West
East
water
sediment
Fig. 6b, c
limestone
sediment and
collapse debris?
limestone
Depth (m)
Distance (m)
Time-domain IP
(b)
(c)
sediment
limestone
296/335
RMS = 9.9%
sediment &
collapse debris?
RMS = 18.7%
Distance (m)
3 10 32 100
ρ (Ωm)
0 1 2 3 4 5 6
−φ (mrad)

Figure 6: Geophysical sections along Profile 3 of Lake Metzabok: (a) sub-bottom profiler section with dashed lines highlighting the main reflector found below the lake floor, dotted lines outlining a zone of high diffuse reflectivity including main reflectors and the dashed box showing the section with TDIP resistivity and phase ~~ERT/IP~~ data, (b) electrical-resistivity image and (c) phase image including electrode positions (black dots along the surface) and lines taken from SBP seismogram. Labels in the lower left corners represent the amount of data points used for the inversion compared to the total measured data (same for resistivity and phase) and the respective percentage root mean square deviations (RMS) of the inversion.

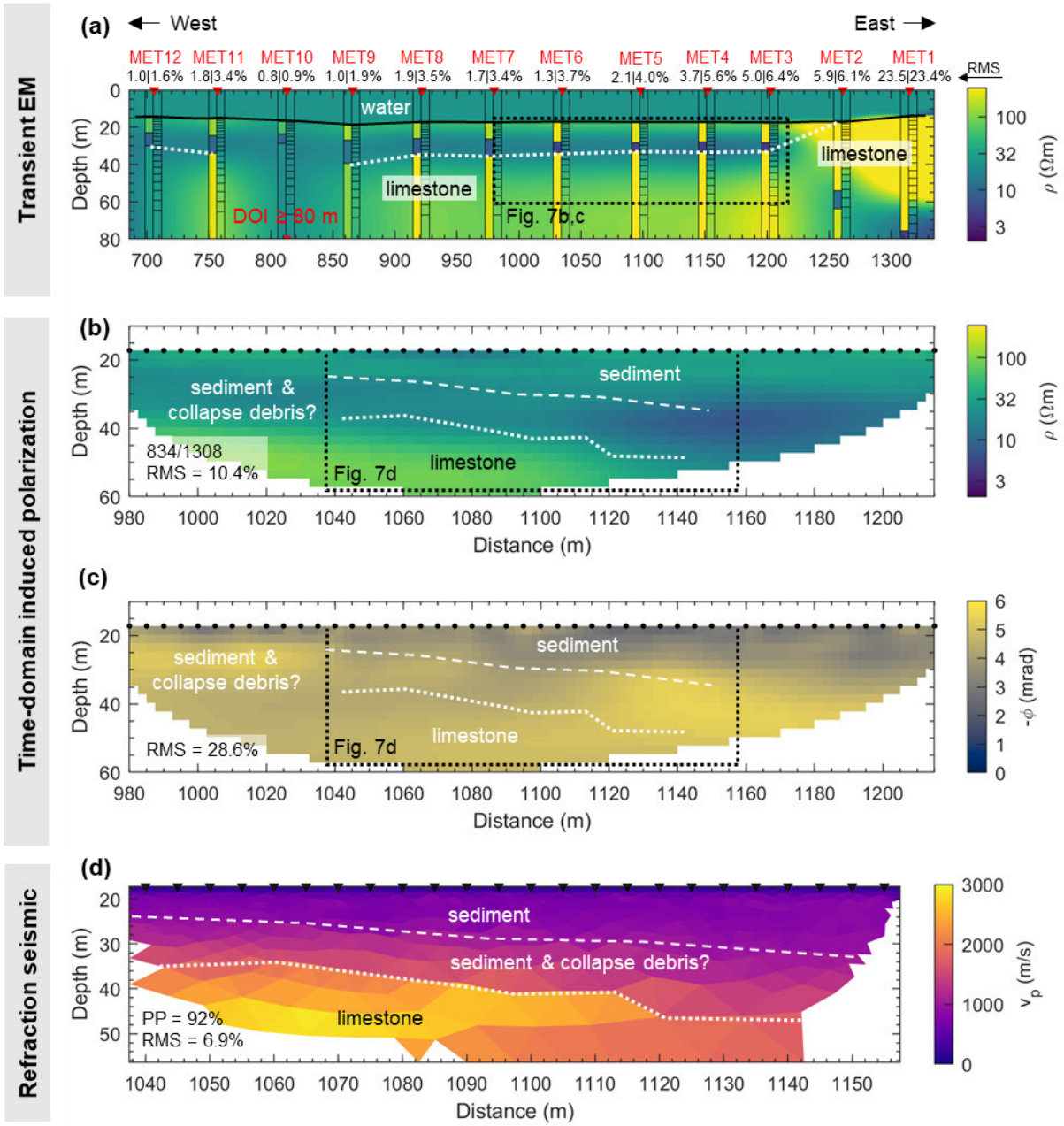

~~**Labels in the lower left corners of the sections refer to the IDs within the data set published along this manuscript.**~~

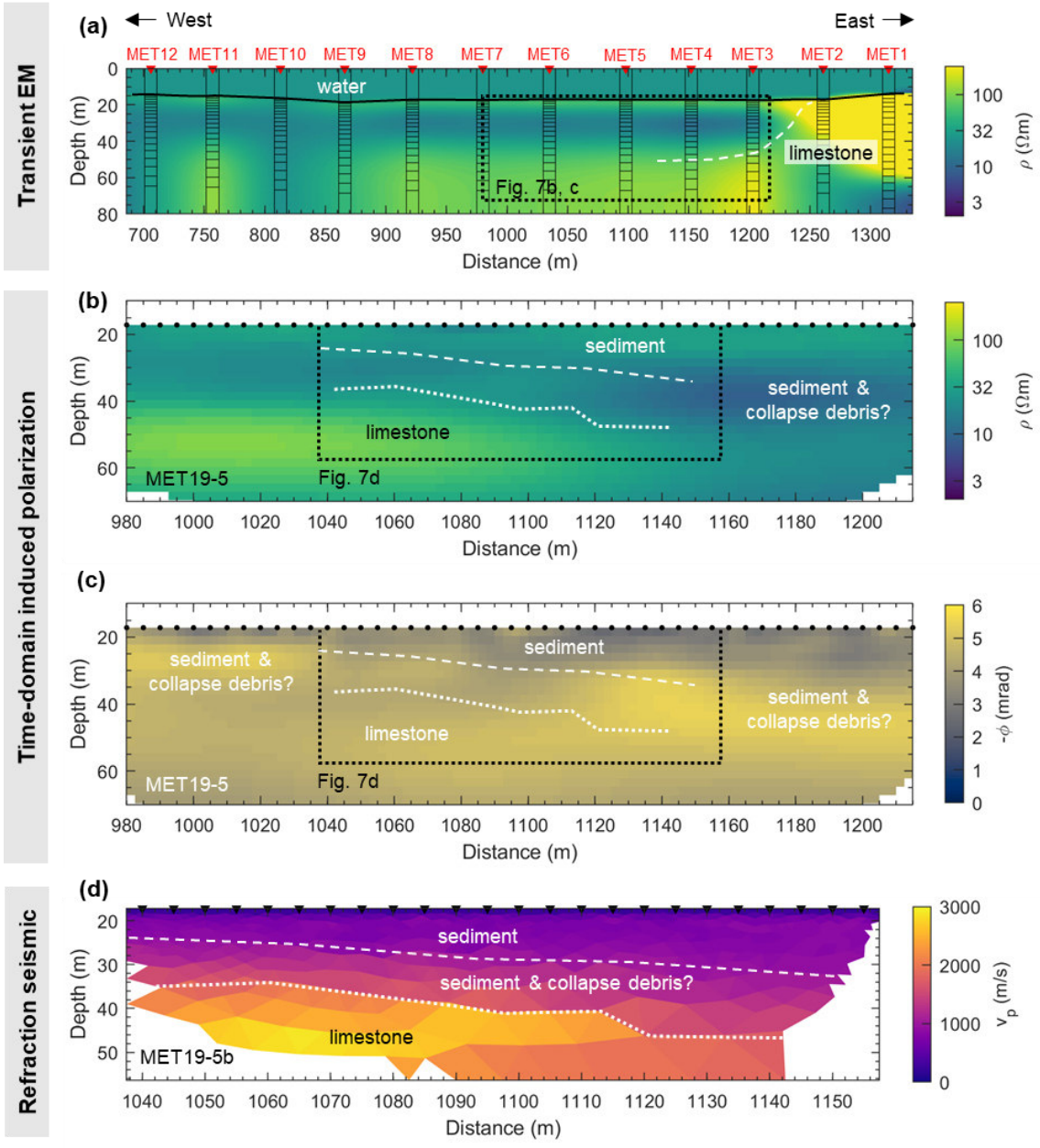

Figure 7: Geophysical sections along Profile 4 of Lake Metzabok: (a) Interpolated TEM image based on ~~TEM image based in~~ smooth 1D models, left bar graphs ~~(bar graphs~~ show layered, right bar graphs smooth models; ~~in the foreground) and interpolated 2D section (background);~~ individual percentage RMS deviations are given for layered and smooth models, respectively. The ~~the~~ black solid line in the section indicates the water-sediment contact, the dotted ~~ashed~~ line the top ~~inferred geometry~~ of the limestone bedrock inferred from this image. **(b)** Eelectrical resistivity and **(c)** phase images including electrode positions (black dots along the surface), and the main lithological units as interpreted from the SRT image in **(d)** (dotted lines). Labels in the lower left corners of (b) and (c) represent the amount of data points used for the inversion compared to the total measured data (same for resistivity and phase) and the respective percentage RMS of the inversion.~~:~~ **(d)** Sseismic refraction tomogram with main lithological units including picking percentage (PP) and RMS of the inversion.

~~. Labels in the lower left corners of the sections refer to the IDs within the data set published along this manuscript.~~

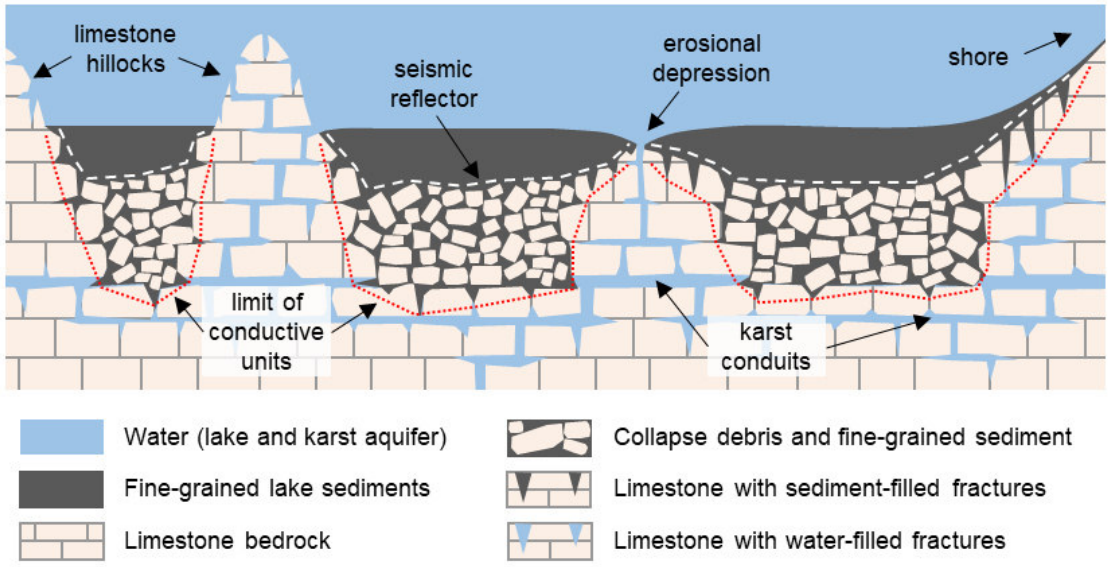
limestone hillocks
seismic reflector
erosional depression
shore
limit of conductive units
karst conduits
Water (lake and karst aquifer)
Fine-grained lake sediments
Limestone bedrock
Collapse debris and fine-grained sediment
Limestone with sediment-filled fractures
Limestone with water-filled fractures

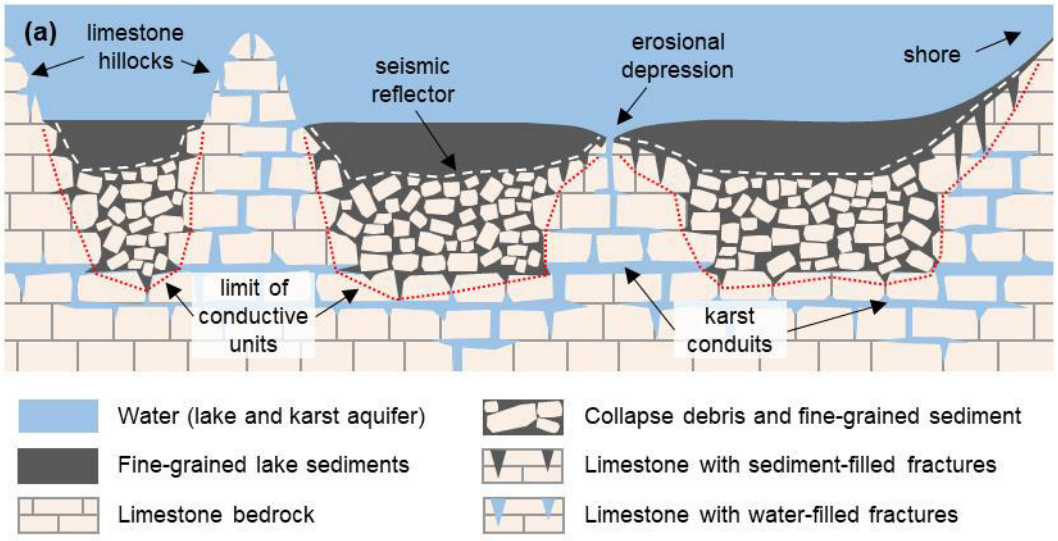
(a)
limestone hillocks
seismic reflector
erosional depression
shore
limit of conductive units
karst conduits
Water (lake and karst aquifer)
Fine-grained lake sediments
Limestone bedrock
Collapse debris and fine-grained sediment
Limestone with sediment-filled fractures
Limestone with water-filled fractures


(b)
(c)
(d)
Fractured limestone
~1.5 m
Fine-grained sediment

900

Figure 8: (a) Schematic sketch summarizing the geological conditions below Lake Metzabok interpreted from the geophysical survey (details not drawn to scale). The limit between the fine-grained lake sediments and the collapse debris with sediment-filled interspaces indicated by the white dashed line stands out as a strong reflector in all sub-bottom profiler images. All units containing fine-grained sediment are characterized by low electrical resistivity values; a strong resistivity increase marks the upper limit of the limestone bedrock as indicated by the red dotted line. Photographs show (b) and (c) limestone debris with fine-grained sediment as well as (d) fractured limestone and fine lake sediments exposed during the low-level stands in October 2019.

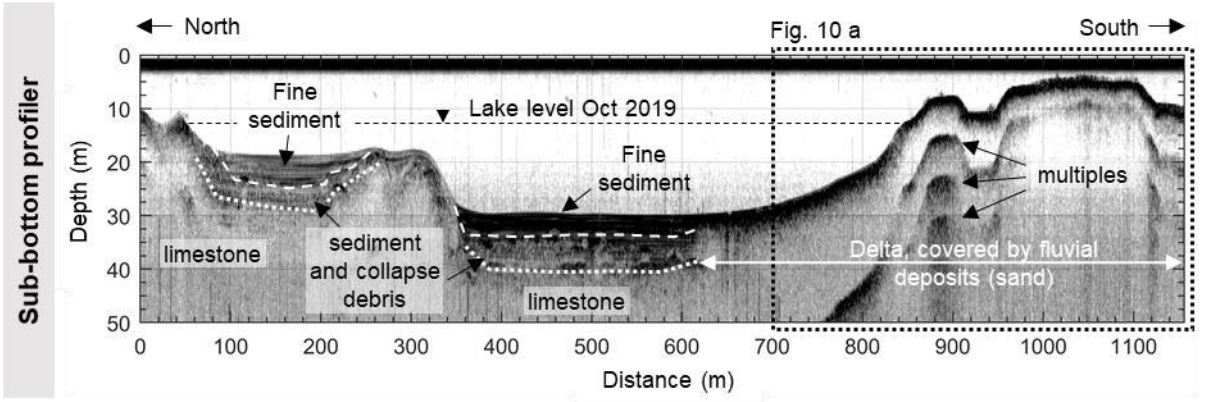

Figure 9: Long N-S oriented sub-bottom profiler section crossing the entire lake Tzibaná (Profile 5). The last approx. 450 m roughly coincide with the TEM section along Profile 6 in Fig. 10a (indicated by the dotted rectangle). The white dashed lines highlight the main reflector below the lake floor, which is interpreted as the lower limit of a fine-grained sediment layer. The white dotted lines enclose the zone of diffuse reflectivity associated with the collapsed, sediment-filled limestone. The black dashed line indicates the approximate lake level during the second field season in October 2020. The last 500 m of the profile correspond to the delta of the Nahá river, where a high reflectivity of the sand-covered lake floor results in the occurrence of strong multiples in the seismogram.

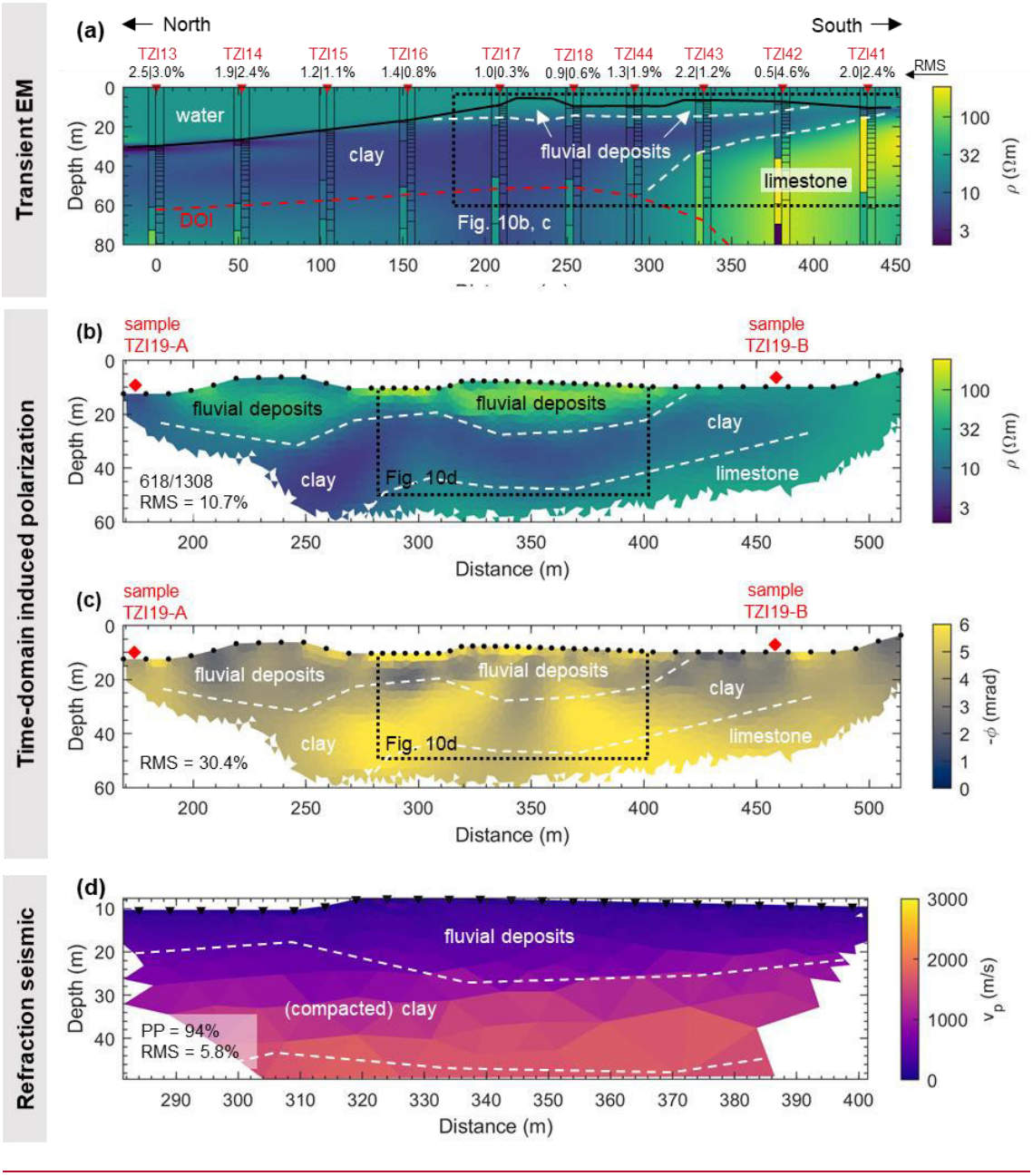
Transient EM
(a)
North
South
TZI13
2.5|3.0%
TZI14
1.9|2.4%
TZI15
1.2|1.1%
TZI16
1.4|0.8%
TZI17
1.0|0.3%
TZI18
0.9|0.6%
TZI44
1.3|1.9%
TZI43
2.2|1.2%
TZI42
0.5|4.6%
TZI41
2.0|2.4%
RMS
water
clay
fluvial deposits
limestone
DOI
Fig. 10b, c
Depth (m)
ρ (Ωm)
Time-domain induced polarization
(b)
sample
TZI19-A
sample
TZI19-B
fluvial deposits
clay
limestone
618/1308
RMS = 10.7%
Fig. 10d
Distance (m)
(c)
RMS = 30.4%
-ϕ (mrad)
Refraction seismic
(d)
(compacted) clay
PP = 94%
RMS = 5.8%
v_p (m/s)

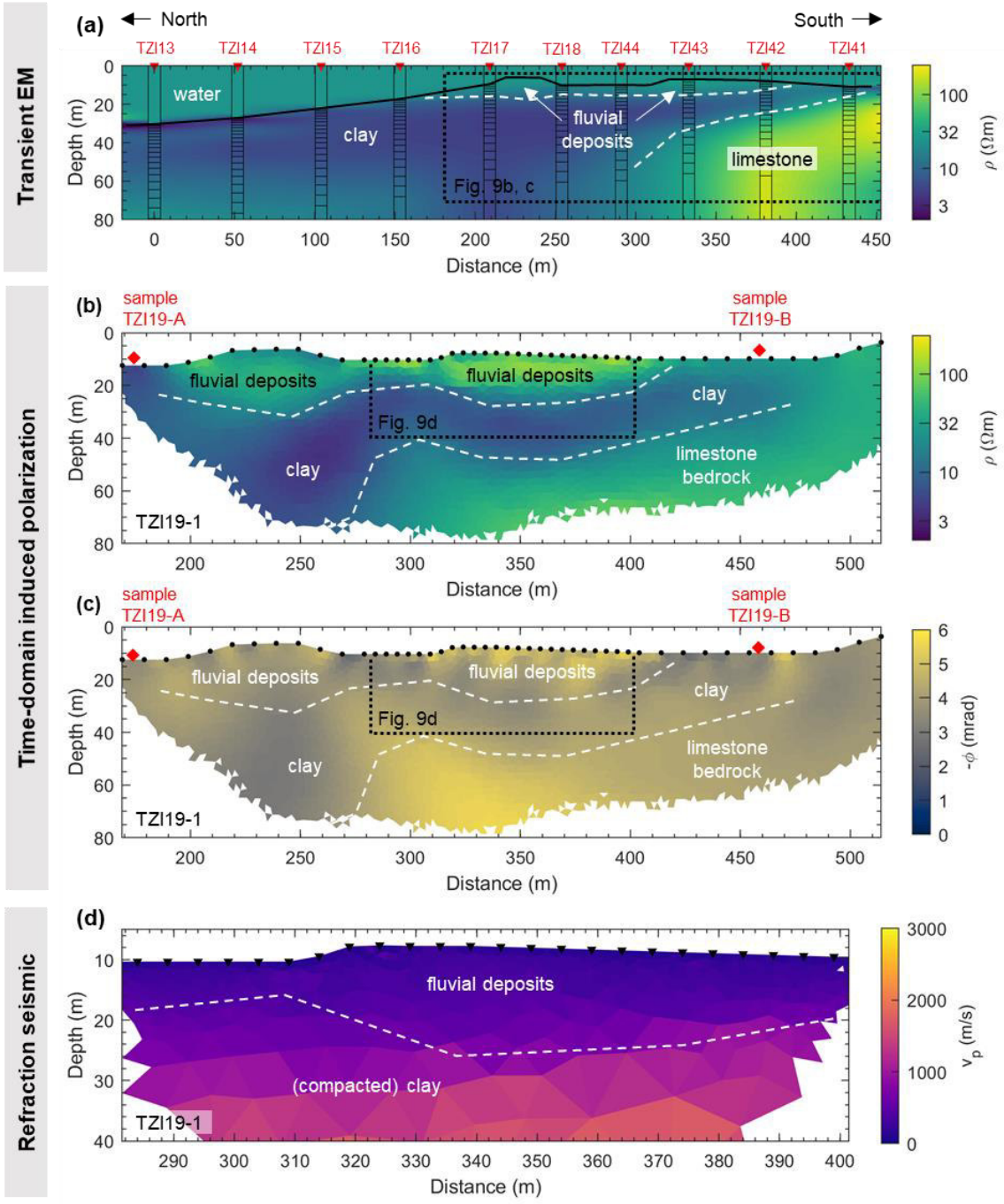

Figure 10: Geophysical sections along Profile 6 of Lake Tzibaná: (a) Interpolated TEM image based on smooth 1D models, left bar graphs show layered, right bar graphs smooth models; individual percentage RMS deviations are given for layered and smooth models, respectively. The black solid line indicates the water-sediment contact, the dashed line the main lithological contacts inferred from this image. (b) Electrical resistivity and (c) phase images including electrode positions (black dots along the surface) and main lithological units. Red diamonds on the surface indicate the location of the sediments sampled for laboratory analyses. Labels in the lower left corners of (b) and (c) represent the amount of

data points used for the inversion compared to the total measured data (same for resistivity and phase) and the respective percentage root mean square deviations (RMS) of the inversion.~~;~~ (d) ~~s~~Seismic refraction tomogram including picking percentage (PP) and RMS of the inversion, contacts of main lithological units (white dashed lines) ~~including the contact between fluvial deposits and clay~~ taken from ~~the~~ TDIP resistivity image. ~~Labels in the lower left corners of the sections refer to the IDs within the data set published along this manuscript.~~

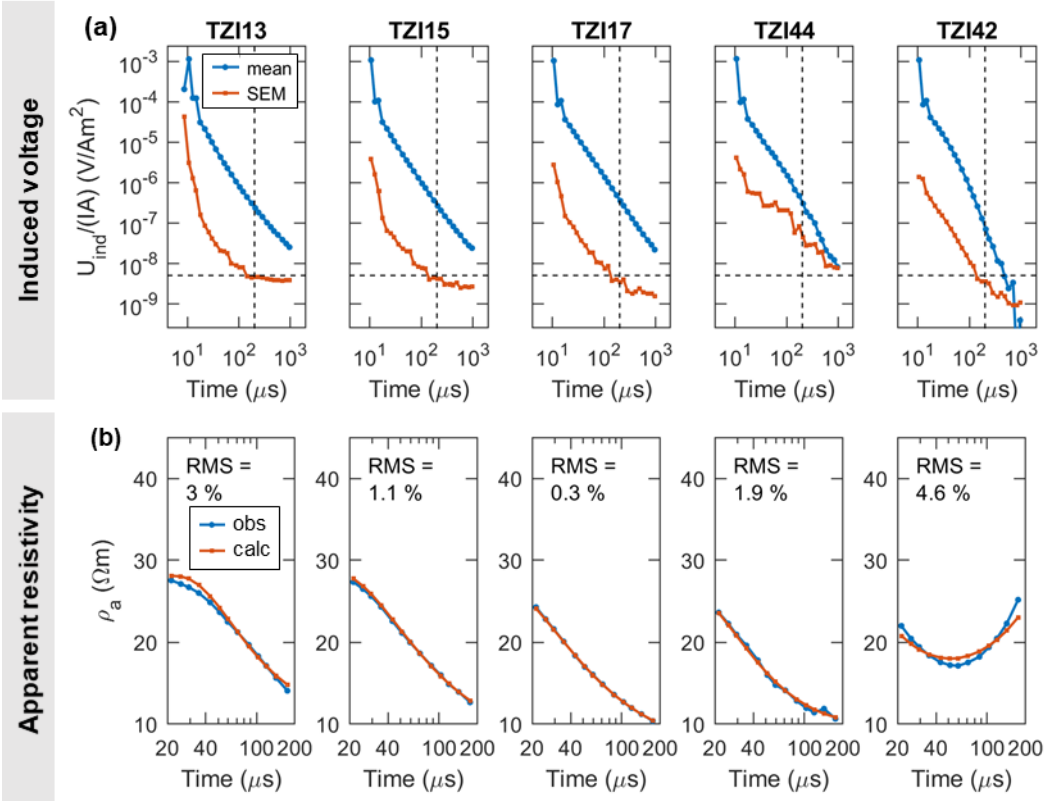

Figure A1. a) Induced-voltage data of selected TEM soundings along Profile 6 of Lake Tzibaná. Induced voltages are normalized with the injected current and the loop area. The mean values of the stacked signal per time gate are shown in blue (circles) the standard error of the mean in red (squares). Dashed lines indicate almost constant (exception: sounding TZI44) late-time error level of $5 \cdot 10^{-9}$ V/Am² (horizontal lines) at 174.5 µs (vertical lines). b) Observed (blue circles) and calculated (red squares) apparent resistivity curves of the same TEM soundings. The root-mean-square (RMS) errors of the individual model fits are indicated, too. The corresponding inverted models (smooth models with 20 layers) are visualized in Fig. 9.

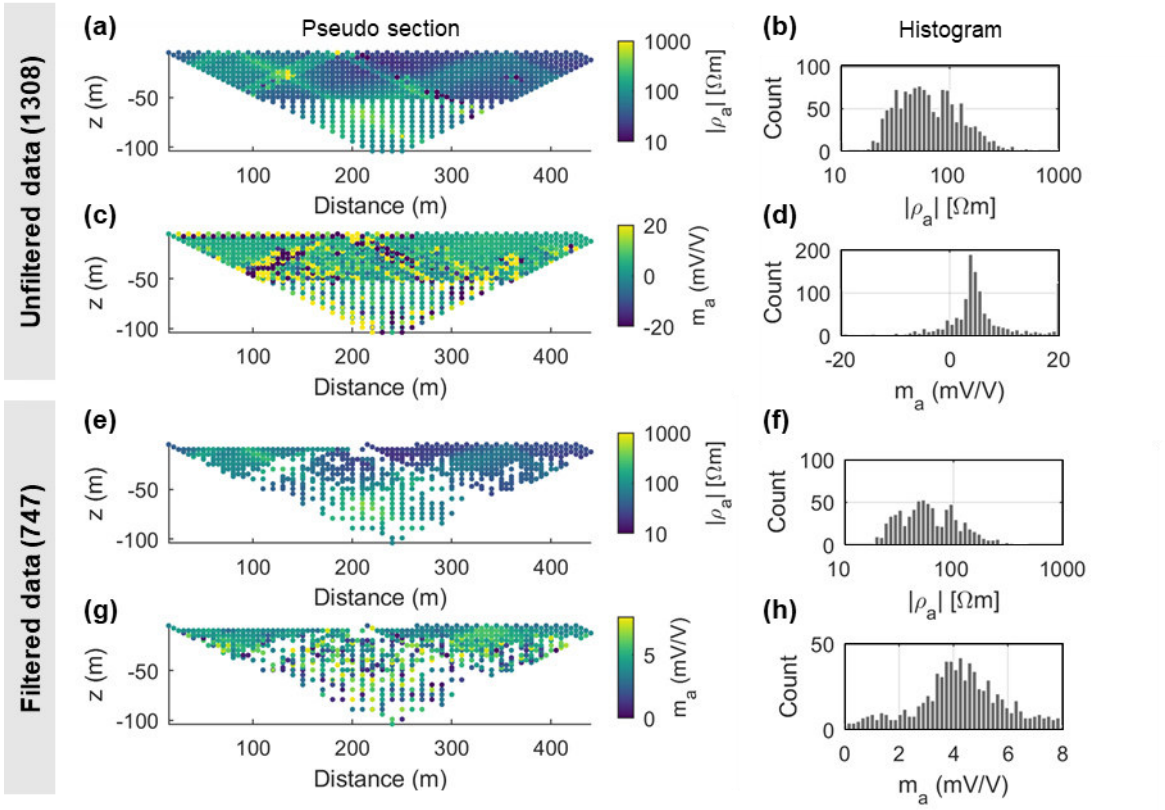

Figure A2. Apparent resistivity and apparent chargeability pseudo sections (left column) and histograms (right column) of the TDIP measurement corresponding to the second part of roll-along Profile 1 of Lake Metzabok. The first two lines (a-d) show the unfiltered raw data set consisting of 1308 individual measurements, the last two lines (e-h) visualize the remaining 747 measurements after the application of the filters described in the main text.

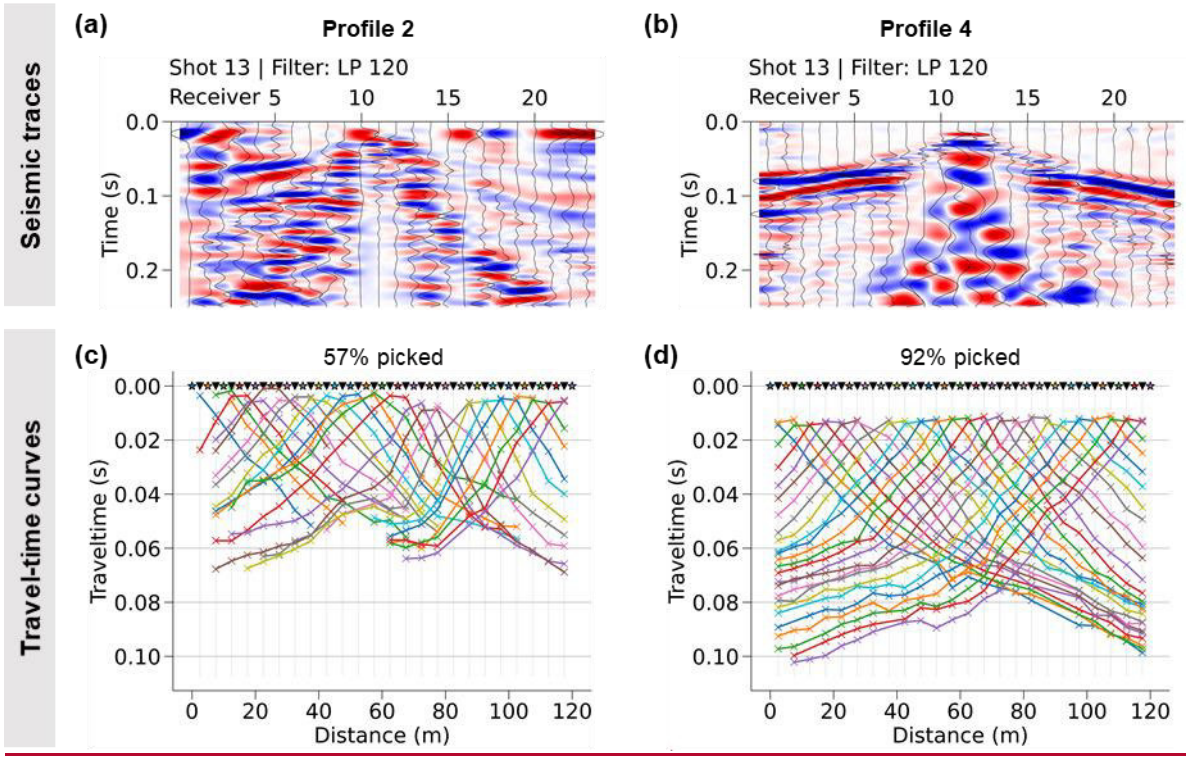

Figure A3. Exemplary seismic traces (wiggle traces with variable density plots in the background) corresponding (a) to Profile 2 with a high noise level and (b) to Profile 4 with a much lower noise level. As a direct result of data quality, the travel-time curves (c) of Profile 2 (picking percentage 57%) are much less populated than those (d) of Profile 4 (92%). The loss of information particularly affects late travel times and thus significantly reduces the depth of investigation along noisy profiles.